Traveling waves and scattering in control of chains

Zdeněk Hurák

November 2015
(Version with corrected typos: October 2016)

Preface

In this text I present my recent research results in the area of distributed control of spatially distributed and/or interconnected dynamical systems. In particular, I approach modeling, analysis and control synthesis for *chains of dynamical systems* by adopting the *traveling-wave* and *scattering* frameworks popular among electrical engineers, and I hope that through this work (and the related publications) I will contribute to (re)introducing these powerful concepts into the control systems engineering community.

The broader domain of spatially distributed systems, into which I include both distributed-parameter systems and interconnected lumped systems, has been recently witnessing a surge of interest among systems and controls researchers. I am no exception because the topic indeed seems to be of growing practical importance due to ubiquitous networking on one side and MEMS technology and lightweight robotics on the other side. Together with my students we have been investigating the topic for the last several years. Mainly we tried to take advantage of the strong footing on the polynomial (or input-output, or frequency-domain) theoretical grounds thanks to our great teachers and colleagues like Vladimír Kučera, Michael Šebek, Jan Ježek and Didier Henrion, who significantly contributed to the development of those techniques in the previous decades. With my students Petr Augusta, Ivo Herman and Dan Martinec we have even succeeded in publishing some of our results in archival journals.

It was only in 2013 that I was made aware of an alternative and not widely popular approach to control of chains of mechanical systems such as masses interconnected with springs and dampers—the traveling wave approach based on the concept of a *wave transfer function* (WTF) as introduced and promoted recently by William J. O'Connor. My former MSc student—Dan Martinec—then a doctoral student supervised by Michael Šebek, was trying to tailor O'Connor's techniques to the vehicular platooning framework. Namely, we was augmenting the popular distributed control schemes based on onboard controllers regulating the distances to the predecessor and possibly the follower, by a *wave absorbing controllers* realized onboard the leading and/or trailing vehicle. His first results looked impressive. The otherwise unsurmountable troubles associated with an amplification of the regulation errors as they propagate along the string (or chain or platoon) of vehicles were tamed with a single onboard feedback controller implemented on the first or the last vehicle. It looked like a magic and I just wanted

to understand the whole approach better. Although the description of the WTF approach in the literature seems to be correct, I kept failing to develop confidence in full understanding of its basic assumptions and limitations. In particular, I was not able to link it to anything that I already knew. Waves in finite dimensional systems? Irrational transfer functions? Furthermore, the concept was intimately linked to the mechanical domain and I love thinking in a multidomain way[1].

This stimulated my curiosity and triggered my research interest in this topic. I was quite lucky that at that moment I was granted a scholarship from Fulbright Program for spending seven months at University of California at Santa Barbara with one of the leading researchers in the research area of distributed control of spatially distributed systems—Bassam Bamieh. This gave me a terrific opportunity to delve deeply in this topic. My motivation was to see if the impressive results obtained within the WTF framework by O'Connor (and some others, including Dan Martinec) can be explained within some standard and well established engineering frameworks, preferably while keeping relevance for several physical domains. My quest brought me pretty soon to the classical electrical engineering topics like *impedance matching* for *transmission lines*, *maximum power transfer*, *conjugate matching*, *paraconjugate matching*, *ladders*, *iterative impedances*, *scattering* and *chain scattering* description. Invoking *Maxwell analogy* among physical domains, these fundamental results found in classic texts for electrical engineers, in particular for microwave specialists, could be easily reinterpreted in the hydraulic, mechanical and other physical domains as well. In fact, what makes these results valid in multiple domains is that they always have a very physical (because energy related) interpretation.

I felt and still feel so fascinated with the new understanding that I wanted to share this with my closest colleagues and students. However, the underlying formalism can be somewhat alien to control systems specialists of these days and therefore I felt a need to provide some background info, perhaps even a tutorial. That is what made me write these notes.

Besides developing and documenting my own understanding of the existing fundamental concepts, I have also succeeded in creating a few original research results. Namely, I have proved some remarkable relationship between the impedance matching for a lossless transmission line and an $\mathcal{H}_\infty$-optimal control design for the same "plant". I investigated the same for the lossless chain (although I could only cast a conjecture based on simulation outcomes) and then related the two. Since the results appear new and original, I decided to use this text as one of the required materials for my habilitation application. While submitting it, two papers are being finalized for a submission to a journal (extracting the essential facts from the two key chapters of this work).

---

[1] I now feel grateful for an opportunity to teach a course on modeling of dynamical systems at CTU in Prague—power bond graphs rule...)

Acknowledgements

Since I have conducted much of the research presented here during my seven-month stay at University of California at Santa Barbara (UCSB) in the spring and the summer 2014 within Fulbright Program, I would like to express my sincere thanks to both Czech and US tax payers, from whom the funding comes. I am doing my best to pay back. I would also like to highlight the very professional job done by the enthusiastic crew of the Fulbright Commission in Prague.

I also feel indebted to my scientific host at UCSB—Bassam Bamieh—for dedicating some of his precious time to scientific discussions with me. I certainly benefited a lot from discussions with his smart students too. I also enjoyed scientific interactions with other members of the internationally well-recognized *Center for Control, Dynamical-Systems, and Computation (CCDC)* at UCSB. In particular, I enjoyed talking science to Igor Mezić and his research team.

Although I did much of this work while at UCSB, there was also some "before" and some "after" and both are related to Department of Control Engineering (DCE) at Faculty of Electrical Engineering at Czech Technical University in Prague. In particular, I would like to thank its head—Michael Šebek— for the long-term support (and patience while waiting for my habilitation...). I also want to thank to some other colleagues at DCE who had to take over my teaching and administrative duties in my seven-month absence. Not surprisingly, the same people have been my closest colleagues during the last years and my scholarly work has benefited a lot from daily interactions with them. In particular, Martin Hromčík and a few graduate students and postdocs from my group, namely Jiří Zemánek, Ivo Herman, Dan Martinec and Kristian Hengster-Movric, to name just those for whom the presented research results might be relevant. After all, my initial motivation to write this work was to share with you, guys, the knowledge I gained and further modestly extended. Join me in pushing this further! Last but not least I would like to Didier Henrion for numerous scientific discussions and also for serving me as a mentor on my academic path.

Contents

Contents

1 Introduction

1.1 Problem statement and motivation

Our goal is to develop a suitable formalism for modeling, analysis and control design for complex dynamical systems with the internal structure as in Fig 1.1.
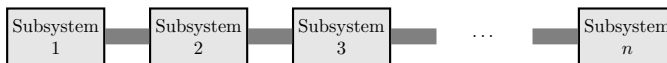
Figure 1.1: Chain of (sub)systems. The dynamics of the subsystems are coupled with the dynamics of their nearest (one or two) neighbors

We are curious to understand how certain properties of the chains scale with the number of subsystems. In particular, we are interested in the *limits of achievable control performance* for very very large chains.

We are going to restrict ourselves to linear systems. While the common arguments goes that the world is nonlinear, there is certainly a lot to learn about fundamental limitations while studying the linear chains.

Let's postpone the definition of the "coupling" among the subsystems after going through a few simple examples of chains from diverse physical domains.

1.1.1 Examples of chains of dynamical systems

In the mechanical domain, consider the notoriously known system composed of multiple masses interconnected with springs and dampers as sketched in Fig. 1.2.
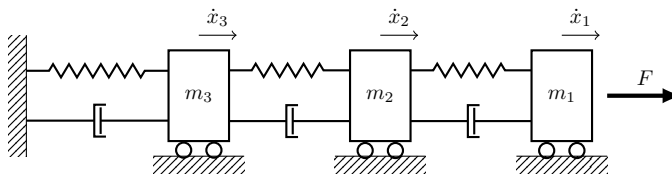
Figure 1.2: Multiple masses interconnected with springs and dampers

Although such simple mechanical chains very often serve just as approximations of a spatially continuous mechanical system, they can also serve as physically justified and relatively accurate models of interconnections of lumped mechanical systems. Examples can be found in flexible serial robotic manipulators or in modeling of tall buildings for the purpose of attenuation of the influence of seismic activities or wind buffets.

In the electrical domain, what we call here the chain structure is more often than not referred to as the *ladder structure* or *cascade interconnection* of two-port networks as in Fig. 1.3, for which the most popular instances are cascades of the
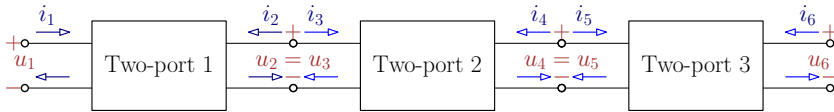
Figure 1.3: Chain (or cascade) interconnection of two-port networks

so-called L- or T- or Π-sections composed of resistors, inductors and capacitors as in Fig. 1.4.
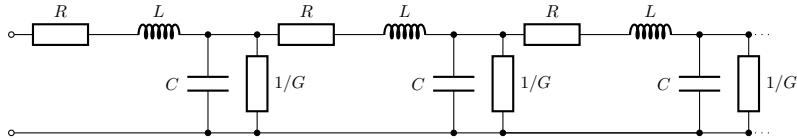
Figure 1.4: An interconnection of a few L-sections (the letter L refers to the topology of the section here) composed of the passive R, L and C components

In hydraulics, the chain model can represent a series of reservoirs and accumulators along a hydraulic pipe such as the one depicted in Fig. 1.5. The level of water in each reservoir is coupled to that of its neighbors, hence the coupling.
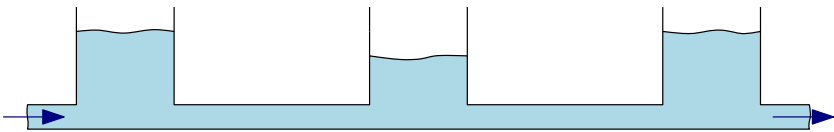
Figure 1.5: Chain of hydraulic accumulators (reservoirs) along a pipe

The coupling between the neighbors in the above chains is apparently of natural physical origin. However, it can also be introduced artificially by a human. As an example consider the vehicular platoon in Fig. 1.6. In its simplest version,

the onboard controller (or a human driver) of each vehicle in the platoon (except for the leader) measures its distance from its nearest neighbors (or at least from its nearest predecessor) and adjusts its throttle so that some prescribed intervehicular distance is kept.
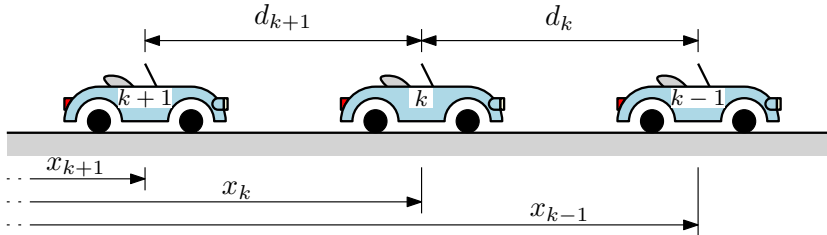
Figure 1.6: Vehicular platoon

1.1.2 Coupling between the neighbors

The gray thick lines in Fig. 1.1 that connect the neighbor subsystems have only been characterized indirectly through the examples. Of course, when it comes to the actual computational realization of the models (state-space models, Simulink graphs, . . .), this two-directional coupling is realized by pairs of *signals*. Based on the examples, these can be force and velocity in the mechanical domain, voltage and current in the electrical domain, pressure and volumetric flow rate in the hydraulic domain, etc. A very natural interpretation of the coupling is then that of *energy (or power) bond* since the product of the variables in the pairs amounts to the rate of transfer of energy—the power.

This interpretation of coupling is certainly not new. I has been widely used in electrical engineering since 1940s or 1950s within the framework of *multiports*. Indeed, through each *port* (implemented by two terminals/wires/leads), the energy is exchanges with the external world. In the late 1950s this was generalized to other physical domains by Henry Paynter in the form of *power bond graphs*. Indeed, the idea that coupling between subsystems has this physical meaning is very appealing from the viewpoint of analysis. And yet, surprisingly, it has not been very much explored in the control theory, the signal-based viewpoint dominates.

In the examples of chains of dynamical systems that we gave above, we have also mentioned one case which does not easily yield to the power bond description— vehicular platooning. The reason is that this coupling can easily be asymmetric. Consider, for example, the very extreme case of asymmetry—each driver (or onboard controller) just senses the distance to the nearest predecessor and presses

the throttle or break pedal so that some prescribed distance is kept. Thus, the behavior of the nearest follower does not influence our driver's decisions—the propagation of signals is clearly one directional. How can this coupling be encoded as an energy exchange? To address this, we will revoke a very powerful framework developed to maturity in some branches of electrical engineering—the so-called *scattering description*, which will allow us to capture even situations with asymmetric coupling within the convenient energy-based framework.

1.1.3 Extensions to spatially multidimensional systems—systems on lattices

In all the examples considered so far, the individual subsystems are ordered in a chain (cascade, ladder, string, . . .), that is, each subsystem can be labeled with an integer index which gives its position in the chain. Thus the resulting composed system can be viewed as *one-dimensional in space*. An immediate extension that comes into one's mind is to consider systems that are two- or three-dimensional. These are also called *systems on lattices*. The motivation can again come both from systems with natural physical coupling (mechanics, even material science) or systems with artificial coupling (formations of autonomous mobile robots or drones). We will not handle these higher-dimensional cases in this work. The extension of some of the results proposed in this work may but need not be straightforward.

1.1.4 Control architectures

For the presented class of interconnected dynamical systems, we consider a suitable control system architecture. The centralized one is described in Fig. 1.7.
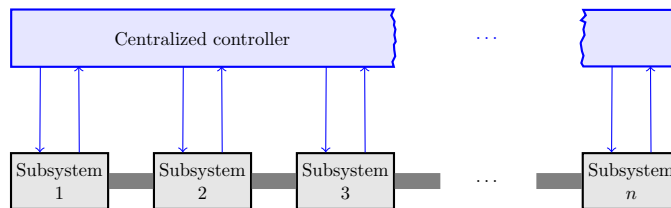
Figure 1.7: Centralized control scheme for a chain of dynamical systems

Although this configuration certainly offers the best achievable control performance, it is very often outruled by complexity of design (too high an order of the model, too many inputs and outputs). Furthermore, from an implementation viewpoint, the requirements on the bandwidth of the communication network

may be prohibitive because all the local measurements need to be brought perpetually to one central controller and similarly the commands produced by the central controller need to be communicated to the subsystems. Vulnerability of such scheme might also be an issue.

The alternatives are the distributed and decentralized control schemes at Fig. 1.8 and 1.9.
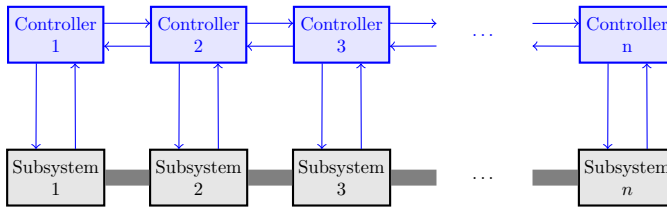
Figure 1.8: Distributed control scheme for a chain of dynamical systems
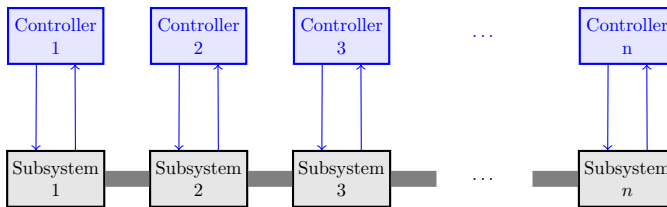
Figure 1.9: Decentralized control scheme for a chain of dynamical systems

The above mentioned two control schemes have been intensively investigated by the control community. Therefore in this text we will focus on yet another scenario—the whole chain is only controlled through a single controller attached to one of the two ends of the chain. This is described in Fig. 1.10.
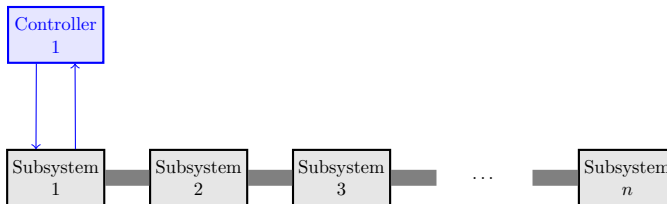
Figure 1.10: Control of a chain of dynamical systems through the ends

Finally, into our framework of coupled systems easily fit systems which are initially without coupling but the coupling is introduced by human designers.

We showed an example of a platoon of vehicles traveling on a highway with tight spacing in Fig. 1.6. The coupling highlighted in the original Fig. 1.1 is implemented as in the block diagram in Fig. 1.11. The realizations of individual coupling controllers can be physically hosted by one of the two participating subsystems. Moreover, the measured variables available to the controllers can be relative (difference in positions, temperatures, etc.).
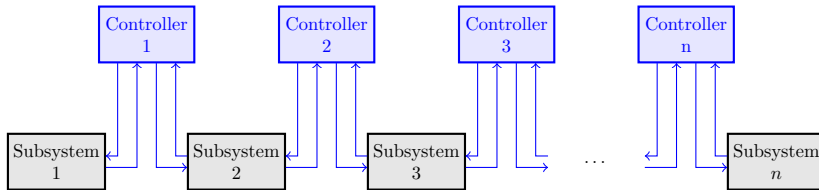
Figure 1.11: Coupling created artificially between the neighbors in a chain of dynamical systems

1.2 State of the art in the control of chains, in particular the traveling-wave approach

The topic of *control of interconnected systems* has been studied extensively by the control theory community for many decades. Among the first motivations in 1960s were vehicular platoons [41], [48], [12]. In particular, it turned out that platoons exhibit a strange behavior as the number of vehicles grows—*string instability* [14], [68].

The new millennium has been witnessing a surge of interest in the theory of interconnected systems, which has been mainly driven by the *networking* permeating all aspects of life and supported by new achievements in mathematical control theory, in particular graph theory. We mention just a few works that highlighted some interesting aspects of control of interconnected/networked/distributed systems, namely [6], [20], [3] and [71].

A prevailing approach to the analysis of distributed systems is based on *modal analysis* popular among mechanical engineers for analysis of flexible structures. The oscillatory behavior of the system is analyzed using *standing waves* (or *modes*). There is, however, an alternative approach which views the response of the systems as a superposition of *traveling waves*. The first application of this approach to analysis and control of flexible mechanical structures appeared in late 1960s in [79]. A significant contribution was done by von Flotow and his students and colleagues in 1980s and is archived in a series of papers such as [81], [80], [50], [82]. An interest of researchers in this topic survived in the new

millennium, as reflected in the work by Halevi [23], [25], [24]. A special issue of the *Mechanical Systems and Signal Processing* journal [11] gives some more papers describing the state of the art as of 2013.

The research in traveling wave approach to control of mechanical structures mimics to some extent the well-established results in electrical engineering, namely, the *transmission line* theory. Indeed, the decomposition of the standing wave into the incident and reflected traveling waves is crucial for devising proper termination of the transmission line—the *(reflection-free) impedance matching*, a classical concept described in numerous texts such as [49], [42] or [69].

The situations in which the transmission medium is not spatially continuous but rather is formed by (cascade) interconnection of lumped sections is studied as well under various names such as *ladder-network delay lines* or *artificial lines* [42] or *analog delay lines*. It is known that if a transmission line is terminated with a load impedance equal to its *characteristic impedance*, the input impedance has the same value. The same concept can be applied to the ladders and such impedance is called an *iterative impedance*. These are typically irrational.

There have been a few adaptations of impedance matching concepts to control analysis and synthesis for interconnected lumped systems. Extension of the "impedance matching based controller" for a heterogeneous mechanical chains (masses interconnected by springs and dampers) is in [65] with an application to vibration control of a multistory building was given in [53]. Reformulation for heterogeneous electric ladder networks is in [52]. The same problem of interconnected mechanical systems was investigated by O'Connor who developed his own framework of a *wave transfer function (WTF)* [59] which does not explicitly relate to the impedance matching issues. A series of papers by the same author followed [58], [62], [56], [57], [62], [55], [60], [61], [63], [64]. In [67] they aim at reconciling the O'Connor's approach with the continuum wave-based control by Halevi. Moreover, they bring in yet another oscillation-suppressing approach into their analysis—*input shaping*, see [73] for a survey.

1.3 My (co-)contribution to the theory of spatially distributed and interconnected systems

The approach to the research topic of spatially distributed and/or interconnected systems has been strongly influence by the background in polynomial (or input-output or frequency-domain or algebraic) techniques. With my doctoral student Petr Augusta we used multivariate (also n-D) polynomials and transfer functions to describe systems with very regular interconnection structure—lattice, see [4] (and a few conference papers). We were not only able to extend some classical techniques such as LQ-optimal control but also incorporate some latest results

for optimization over positive polynomials. With Michael Šebek we then applied these techniques to analysis of vehicular platoons [31]. However, it turned out that even though the n-D transfer function description is very compact (just consider the neatness of the transfer function $G(s, z) = \frac{z^{-1}-1}{ms^2}$ of a however long vehicular platoon with a predecessor following control strategy), the analysis is far from trivial. The reason is that some standard results for 1-D polynomials and 1-D transfer functions do not extend easily to their n-D counterparts. Even the most fundamental concepts such as stability and coprimeness become very contrived and mastery of the theory of complex functions of several variables is a must. That is why I abandoned this approach, at least temporarily.

In the meantime, another doctoral student—Ivo Herman—whom I have been co-advising with Michael Šebek—has continued using polynomial and transfer function techniques but combined them with some classical results from algebraic graph theory. In particular, in the paper [27] published in IEEE TAC we show that the nonzero bound on the second smallest eigenvalue of the graph Laplacian, which was once praised as a good quality of an asymmetric platoon, signals very bad (exponential) scaling of the platoon as the number of vehicles grows. The impact of asymmetry is further elaborated in [28] (already accepted for IEEE TAC).

With Dan Martinec, while a MSc student, we built a few experimental demos for vehicular platooning. First, using just some ten boxes of the popular Lego Mindstorms NXT to build a platoon of ten autonomous vehicles traveling as a platoon [44]. Second, building a significantly more agile platoon of vehicles using Carrera slotcars and our own hardware that turned the dull toys into autonomous machines with sufficient computational power [45]. We still continue with this experimental platform, see the webpage `http://aa4cc.dce.fel.cvut.cz` or the "aa4cc" Youtube channel for some videos.

Later, Dan Martinec, while a PhD student advised by Michael Šebek, tailored the O'Connor's *wave transfer function* approach to bidirectional control of vehicular platoons and we describe this in [46].

Finally, with another doctoral student of mine—Jiří Zemánek—we have been working on a novel approach to (micro)manipulation which is based on shaping the electric or magnetic field through a large array of actuators (electrodes for the electric field and coils for the magnetic one). One of our early descriptions of the problem from the viewpoint of control theory is in [30]. Recent report on experimental achievements is in [86]. This research problem nicely combines both the spatially continuous "physics" and the spatially discrete actuation and possibly even sensing and control logic.

1.4 Outline of the work

The next chapter is dedicated to spatially continuous systems. Namely, I start by giving a short intro to the problem of reflection-free impedance matching for transmission lines. Then I reformulate the problem in the language of control theory using the popular framework of linear fractional transformation (LFT) and I show that this leads to a very unusual control design task consisting in solving a quadratic (in the controller's transfer function) equation. Finally, I relate this unconventional control design to the widely popular $\mathcal{H}_\infty$-optimal control design and show that for lossless transmission lines these are identical.

   This result may be of some interest on its own because many physically relevant phenomena can be described by a wave equation (hence the transmission line model) but my major motivation was to understand better the *limits* of the designs to be done in the subsequent chapter. Namely, that chapter is dedicated to spatially discrete systems—ladders or chains. Mimicking the development of the well-understood reflection-free impedance matching of transmission lines brings us to a related concept of an iterative impedance. After examining it closely, I again aim at finding the relationship with the the $\mathcal{H}_\infty$-optimal control design. Then I discuss how these results, which were derived for the electrical circuits and networks systems, could be applied in other physical domains, thanks to analogies among physical domains. Namely, I show how these could be interpreted for the mass-spring-damper chains. After this discussion I show how the presented results on matching and iterative impedances related to the *wave transfer function* concept, which essentially triggered my interest in the topic.

2 Spatially continuous medium—transmission line theory

2.1 Introduction

In this introductory section we start by recalling a few basic terms and concepts from both control and circuit theory so that we can later state the motivation and goals of this chapter.

2.1.1 Linear fractional transformation and $\mathcal{H}_\infty$-optimal control

Linear fractional transformation (LFT) within the control systems framework denotes the feedback interconnection of a plant (the system to be controlled) and a controller in Fig. 2.1.
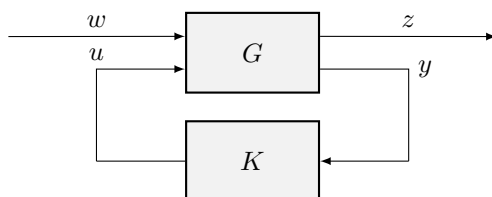
Figure 2.1: Lower linear fractional transformation of a generalized plant (described by a matrix transfer function G) with respect to the controller (with a transfer function K)

The linear(ized) model of the (generalized) plant comes in the form of a matrix transfer function $G(s)$ structured as

$$G(s) = \begin{bmatrix} G_{11}(s) & G_{12}(s) \\ G_{21}(s) & G_{22}(s) \end{bmatrix}. \tag{2.1}$$

This structure is given by classifying the inputs into two groups: exogenous input(s) w and control input(s) u, and the outputs into: regulated output(s) z and measured output(s) y. In this work we will only consider scalar signals

w, u, z and y, hence the matrix transfer function G will be of size 2×2. A linear controller is described by its transfer function K. The closed-loop transfer function F from the exogenous signal w to the regulated variable z is given by the *lower LFT* (labeled $\mathcal{F}_{\text{lower}}(\cdot, \cdot)$ in equations) of G with respect to K

$$F = \mathcal{F}_{\text{lower}}(G, K) = G_{11} + G_{12}K\left(I - G_{22}K\right)^{-1}G_{21}, \qquad (2.2)$$

which in our scalar case simplifies to

$$F = G_{11} + \frac{G_{12}KG_{21}}{1 - G_{22}K}. \qquad (2.3)$$

After identifying properly all the four signals and building the (generalized) plant description, the control design can be cast as an optimization problem: find the feedback controller that not only stabilizes the feedback loop but also makes the transfer function from w to z optimal *in some sense*.

One popular optimization framework is that of minimizing the $\mathcal{H}_{\infty}$ norm of the closed-loop system, that is,

$$\text{minimize} \left\|\mathcal{F}_{\text{lower}}(G, K)\right\|_{\infty}, \qquad (2.4)$$

over K stabilizing. Stabilization means that the closed-loop transfer function F resides in the space $\mathcal{H}_{\infty}$ of functions that are analytic and bounded in the (extended) complex right half-plane. The $\mathcal{H}_{\infty}$ norm of a scalar transfer function $F(s)$ is defined as

$$\|F\|_{\infty} = \sup_{\omega \in \mathrm{R}} |F(j\omega)|. \qquad (2.5)$$

This norm also serves as the worst-case gain for the 2-norms of the corresponding time-domain input and output signals

$$\|F\|_{\infty} = \sup_{w \setminus \{0\}} \frac{\|z\|_2}{\|w\|_2}. \qquad (2.6)$$

2.1.2 Impedance matching

There are two related yet distinct notions of impedance matching used by engineers. We will review them first and then comment on their relationship.

Reflection-free (or reflectionless or zero-reflection) impedance matching for a transmission line

A standard situation encountered by electrical engineers is in Fig. 2.2, wherein a (long) pair of closely spaced cables—a transmission line—is used to deliver a signal (or a power, depending on the context) to a receiver (or a load). The material
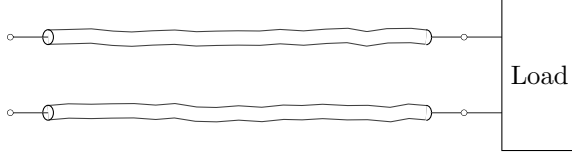
Figure 2.2: Transmission line loaded on one port

reviewed here can be found in texts on microwave engineering and transmission lines such as [69], [49] or [42]. But nice exposition of the basics can also be found in the control-oriented textbook [18], which also supports the use of analogies among the physical domains.

Even if the losses in the cables are negligible, it is generally not possible to neglect the dynamics of the transmission line. The voltage and current are then parameterized by the position x along the transmission line, that is, we have to consider $u(x, t)$ and $i(x, t)$. A linear model of a lossless transmission line is

$$
\begin{aligned}
\frac{\partial u(x,t)}{\partial x} &= -L\,\frac{\partial i(x,t)}{\partial t}, \\
\frac{\partial i(x,t)}{\partial x} &= -C\,\frac{\partial u(x,t)}{\partial t},
\end{aligned}
\tag{2.7}
$$

where L and C are unit-length inductance and capacitance, respectively.

The two PDEs (2.7) constitute one possible realization of the classical wave equation

$$
\frac{\partial^2 u(x,t)}{\partial x^2} = \frac{1}{c^2}\,\frac{\partial^2 u(x,t)}{\partial t^2},
\tag{2.8}
$$

where the velocity coefficient is given by

$$
c = \frac{1}{\sqrt{LC}}.
\tag{2.9}
$$

The wave character of the (model of the) transmission line suggests that in agreement with the d'Alembert's solution of the wave equation, both the voltage and current at any place can be expressed as a composition of *incident* and *reflected (traveling) waves*, indexed with $+$ and $-$ indices, respectively, as in

$$
u(x,t) = u^+(x,t) + u^-(x,t),
\tag{2.10}
$$

$$
i(x,t) = i^+(x,t) - i^-(x,t).
\tag{2.11}
$$

The incident wave travels towards the loaded termination, the reflected wave then travels back.

For the lossless transmission line, the condition of no reflection at the end (on the load side) is that the load impedance must be matched to the *characteristic impedance* of the transmission line

$$Z_{\mathrm{L}}(s) = Z_{\mathrm{c}}(s), \qquad (2.12)$$

where the characteristic impedance of a transmission line is a ratio between the Laplace transformed voltage and current, $\hat{u}(x, s)$ and $\hat{i}(x, s)$, respectively, for the fictitious situation of a transmission line of an infinite length. This assumption of an infinite length assures that there are no reflections at the end of the line (there is no end at all). Thus

$$Z_{\mathrm{c}}(s) = \frac{\hat{u}^{+}(x, s)}{\hat{i}^{+}(x, s)}. \qquad (2.13)$$

For the lossless line the characteristic impedance is just a constant

$$Z_{\mathrm{c}} = \sqrt{\frac{L}{C}}. \qquad (2.14)$$

A transmission line loaded with the matching impedance is called *flat* because for a constant voltage applied across the driving terminals, the voltage remains constant all along the line. This would not be the case for an unmatched transmission line, where oscillations (standing waves) could be observed as a demonstration of superposition of the incident and reflected waves.

Maximum power transfer (conjugate) impedance matching

A setup for another concept of impedance matching is in Fig. 2.3—an interconnection of a (voltage) generator and a load. According to Thévenin's theorem, a real generator of voltage can be represented as a series interconnection of an ideal generator of voltage e_G and an internal impedance Z_{G}. The task is to choose the load such that the maximum possible power is transferred from the generator to the load. This is known as the *Maximum Power Transfer* problem (see, for example [7], [37], [13] or essentially any textbook on electric networks/circuits).
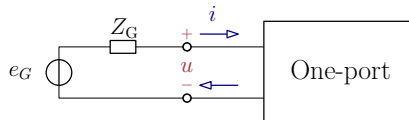

Figure 2.3: A load attached to a generator with an internal impedance

If the generator is producing a harmonic voltage $e_{\mathrm{G}}(t) = e_{\mathrm{G,m}} \cos(\omega_0 t + \phi)$ at a given frequency ω_0, then in order to deliver as much power as possible from the generator to the load, the two impedances must satisfy the

$$Z_{\mathrm{L}}(\jmath\omega_0) = \overline{Z_{\mathrm{G}}(\jmath\omega_0)}, \tag{2.15}$$

where the bar denotes complex conjugation. Hence the name—*conjugate matching*. If several frequencies are contained in the generator's output, the conjugate matching condition must be satisfied for all of them. This makes it generally difficult to do a broadband conjugate impedance matching (note that for a given passive impedance, its conjugate impedance is not passive any more).

If the internal impedance is real, that is, $Z_{\mathrm{G}} = R_{\mathrm{G}}$, the condition simplifies to

$$(Z_{\mathrm{L}} =)\, R_{\mathrm{L}} = R_{\mathrm{G}}, \tag{2.16}$$

where R_{L} and R_{G} are the load and the internal generator resistances, respectively.

Although with the load resistance made identical to that of the generator, the maximum power is transfered from the generator to the load, one half of the power is still "burnt" on the internal resistor. The power transferred to an arbitrary (real) load is

$$\mathcal{P}(t) = u(t)\,i(t) = e(t)\frac{R_{\mathrm{L}}}{R_{\mathrm{L}} + R_{\mathrm{G}}}\frac{e(t)}{R_{\mathrm{L}} + R_{\mathrm{G}}}, \tag{2.17}$$

which for $R_{\mathrm{L}} = R_{\mathrm{G}}$ gives the maximum value

$$\mathcal{P}_a(t) = \frac{e^2(t)}{4R_{\mathrm{G}}}. \tag{2.18}$$

This is the best that could be achieved, thus this power is also called *available power* (hence the subscript). For all other choices of the load impedance, even more power will be dissipated on the internal generator resistor.

Beware that the condition of conjugate matching is valid for harmonic generators only. This constraint might be easily overlooked in the texts on electrical circuits. As a matter of fact, we can only find a discussion of generalization of this condition in [37], page 290. For rational impedances with real coefficients, the condition reads

$$Z_{\mathrm{L}}(s) = Z_{\mathrm{G}*}(s), \tag{2.19}$$

where $Z_{\mathrm{G}*}$ is called *paraconjugate* of Z_{G}

$$Z_{\mathrm{G}*}(s) = Z_{\mathrm{G}}(-s). \tag{2.20}$$

and on the imaginary axis it agrees with the complex conjugate.

Relationship between the reflection-free and the maximum power transfer impedance matching

The two concepts of impedance matching are fundamentally different. The *reflection-free impedance matching* is conditioned by the local properties of medium in which the wave is transmitted (the transmission line here) and its boundary or termination, be it on the load side or the generator side. Whether or not the voltage (or current) wave is reflected on load side does not depend at all on the impedance matching (or any other condition) on the generator side. On the other hand, the conjugate (or paraconjugate) impedance matching deals with the relationship between the generator and the load. If a transmission line is used to connect the two, its model becomes part of the model of the load or the generator for the purpose of analysis.

For example, with the setup in Fig. 2.4 and with $Z_L = Z_c = 1$, $Z_G = 2$, one can prevent reflections of voltage (or current) waves at the load side and yet in this setup the transfer of power from the generator to the load will not be optimal.
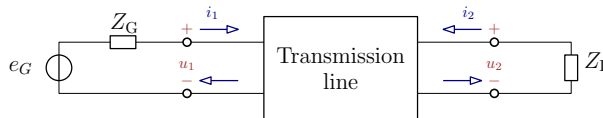
Figure 2.4: Interconnection of a voltage generator, a transmission line and a load

It is unfortunate that in many textbooks this distinction is not discussed in a sufficient depth. A nice exception is [69]. Perhaps what adds to the potential confusion is the fact that in the case of a real generator impedance and a loss-less transmission line, both conditions come in the form of an equality of two resistances, which conceals the fact that they are fundamentally two different concepts. A similar complaint appeared recently in a clarifying tutorial paper [84]. Another nice exposition is [70]. Both papers revolve around comparing *scattering description* and *power waves*, which we will only lightly touch upon towards the end of the chapter.

Some authors like [37] or [54] attempted to reconcile the two impedance matching concepts by formally interconnecting the generator and the load with a transmission line of zero length when investigating the maximum power transfer impedance matching.

2.1.3 Impedance matching as linear fractional transformation

Analysis of a transmission line benefits from treating it as *two-port network*. That is, we will only consider its voltage-current pairs at the left and right ends. We assign the position of the the generator side of the transmission line to $x = 0$ and

the position of the load side to $x = l$, where l is the length of the transmission line. For convenience we label the corresponding *port variables* as

$$u_1(t) := u(0, t), \tag{2.21}$$
$$i_1(t) := i(0, t), \tag{2.22}$$
$$u_2(t) := u(l, t), \tag{2.23}$$
$$i_2(t) := i(l, t). \tag{2.24}$$

With two equations, only two out of the four variables can be independent, that is, two of the four variables can be considered as the inputs while the other two will be the responses or the outputs. Hence we can find a number of combinations leading to a number of formats of models. One particular choice considers u_1 and i_1 as the inputs. This is called an *inverse hybrid model*, also *g*-parameters

$$\begin{bmatrix} \hat{i}_1(s) \\ \hat{u}_2(s) \end{bmatrix} = \underbrace{\begin{bmatrix} G_{11}(s) & G_{12}(s) \\ G_{21}(s) & G_{22}(s) \end{bmatrix}}_{G(s)} \begin{bmatrix} \hat{u}_1(s) \\ \hat{i}_2(s) \end{bmatrix}, \tag{2.25}$$

where *hat* denotes Laplace transform of the corresponding time-domain signal and G can be determined by solving the set of equations (2.7), which yields

$$G(s) = \begin{bmatrix} \frac{\tanh(\sqrt{LC}ls)}{Z_c(s)} & -\mathrm{sech}\left(\sqrt{LC}ls\right) \\ \mathrm{sech}\left(\sqrt{LC}ls\right) & \tanh\left(\sqrt{LC}ls\right) Z_c(s) \end{bmatrix}. \tag{2.26}$$

The interconnections in the "physical diagram" in Fig. 2.5 can be redrawn in
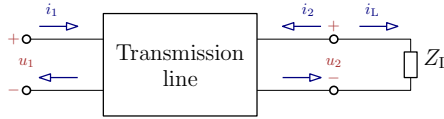
Figure 2.5: Transmission line represented as a two-port network loaded on one port with an impedance Z_L

a signal-flow diagram as in Fig. 2.6.

The relationship between this signal-flow diagram and the lower LFT in Fig. 2.1 is now imminent, although one must not overlook that because of the conventions that currents are entering the port, the feedback loop must be negative. The loaded transmission line becomes a one-port network and its *admittance* (the inverse of impedance)

$$Y_1(s) = \frac{\hat{i}_1(s)}{\hat{u}_1(s)} \tag{2.27}$$
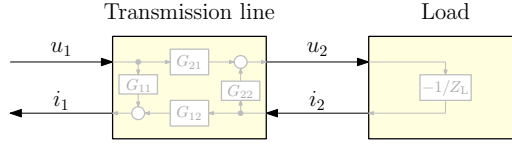
Figure 2.6: Signal-flow diagram of an interconnection of a two-port network described with an inverse hybrid transfer function and a load described with an admittance

can be computed using

$$Y_1 = \mathcal{F}_{\text{lower}}(G, Y_L) = G_{11} - \frac{G_{12}Y_L G_{21}}{1 + G_{22}Y_L}. \tag{2.28}$$

Combining this with the inverse hybrid description of the two-port network in (2.26), we get

$$Y_1(s) = Y_c \frac{Y_L(s) + Y_c \tanh(l\gamma(s))}{Y_c + Y_L(s) \tanh(l\gamma(s))}, \tag{2.29}$$

where $\gamma(s) = \sqrt{LC}s$ and the characteristic admittance is given by

$$Y_c = \frac{1}{Z_c} \left(= \sqrt{\frac{C}{L}} \right). \tag{2.30}$$

We have already recapped that in order to prevent the incident voltage and current waves from reflections on the load, the load admittance must be real and must satisfy

$$Y_L = Y_c. \tag{2.31}$$

We can arrive at an insightful interpretation of reflection-free impedance matching upon evaluating the input-port admittance Y_1 for the line terminated with a matching load, namely

$$Y_1 = Y_L, \tag{2.32}$$

and, of course,

$$Z_1 = Z_L. \tag{2.33}$$

In words, the matched transmission line seems transparent from the input port, the only admittance (or impedance) that can be "seen" at the input port is that of the load. This invites to exploit this equality in the LFT (2.28) for the loaded transmission line

$$Y_L = G_{11} - \frac{G_{12}Y_L G_{21}}{1 + G_{22}Y_L}. \tag{2.34}$$

This is a quadratic equation in Y_L

$$G_{22}\, {Y_\mathrm{L}}^2 + (1 + G_{12}\, G_{21} - G_{11}\, G_{22})\, Y_\mathrm{L} - G_{11} = 0. \tag{2.35}$$

Substituting for G into the general solution of a second-order equation we get

$$\begin{aligned}
Y_\mathrm{L,matched} = &\frac{-(1 + G_{12}\, G_{21} - G_{11}\, G_{22})}{2G_{22}} \\
&\pm \frac{\sqrt{(1 + G_{12}\, G_{21} - G_{11}\, G_{22})^2 + 4G_{11}\, G_{22}}}{2G_{22}},
\end{aligned} \tag{2.36}$$

wherein the irrational part disappears and after some tedious manipulations one can show that

$$Y_\mathrm{L,matched}(s) = \pm\sqrt{\frac{C}{L}} \quad \left(= \pm\frac{1}{Z_\mathrm{c}}\right). \tag{2.37}$$

The fact that we have now discovered two solutions may come at surprise but the new solution, having a negative value of resistance, can be interpreted as an *active* solution. Indeed, a *negative impedance* is a well-known concept in electrical circuits and is used to represent a special type of a source that sets its voltage based on the current that flows through it (or sets its current based on the voltage across its terminals).

2.1.4 Traveling waves and impedance matching in control

There are diverse physical phenomena in numerous engineering applications, which exhibit the wave dynamics as sketched above. Instead of viewing the oscillations in the systems as demonstration of a *standing wave* (and following the well-established *modal* analysis), it sometimes turns out useful to decompose the standing wave into two *traveling waves* going in the opposite directions. The special issue of the *Mechanical Systems and Signal Processing* journal [11] gives some up-to-date overview, although somewhat biased towards flexible mechanical structures. See [81], [50], [25], [74] for some more examples of analysis of flexible mechanical structures through traveling wave approaches. The traveling wave viewpoint also proves useful in studying propagation of electromechanical disturbances in large and dense (hence could be approximated by a continuum model) power generation and distribution networks, see for instance [72], [75] and [40]. Perhaps surprisingly, the wave approach was successfully used to compensate for the detrimental effect of time delays in bilateral teleoperation of robots [2], [29]. There are also control design challenges in acoustic and thermoacoustic domains where the traveling wave might yield some more insight [19].

Although these systems typically span two- or three-dimensional spatial domains, some lesson can be learned by restricting attention to the one-dimensional case.

If control is only allowed through the boundaries, the concept of *impedance matching* offers itself as one suitable framework. The motivation for our work is to see how this practical concept (or concepts) of impedance matching fit into the framework of optimal control theory. Namely, we are going to show that in the case of a lossless transmission line, the standard and relatively easy task of terminating the line with a matching (real) impedance is equivalent to the much more computationally involved task of finding an $\mathcal{H}_\infty$-optimal controller for an infinite-dimensional system.

2.2 Control theoretic formulation of impedance matching within LFT framework

2.2.1 Reflection-free impedance matching

We can recognize the task of finding the matching load impedance (admittance) for a transmission line in Fig. 2.6 as a special instance of the generalized feedback control design problem within the LFT setting as in Fig. 2.1. We will now make a switch to the notational conventions favored by the control theory community: we rename the load admittance Y_L into the "controller" K

$$K := Y_\mathrm{L} \tag{2.38}$$

and instead of the input-port admittance Y_1 of the loaded transmission line we are going to speak about the closed-loop transfer function F (note however that we opted to use the conventions that force us to use a negative feedback)

$$F := \mathcal{F}_{\mathrm{lower}}(G, -K). \tag{2.39}$$

The control-theoretic translation of the impedance matching requirement (2.32) turns out somewhat nontraditional: find a stabilizing feedback controller K such that

$$K = \mathcal{F}_{\mathrm{lower}}(G, -K). \tag{2.40}$$

In words, find a stabilizing feedback controller that yields the closed-loop system with the identical transfer function! This is not quite a usual control design problem, is it? Most often than not, the control design problems formulated in the LFT framework lead to an optimization of some closed-loop characteristic such as $\mathcal{H}_1$, $\mathcal{H}_2$ and ℓ_1 system norms. The question that will keep us busy till the rest of the chapter is whether the impedance-matching "controller" is optimal in any such usual (or unusual) sense.

2.3 Static $\mathcal{H}_\infty$-optimal control problem for a lossless transmission line

For convenience we start our analysis using a model (2.29) of a transmission line with *normalized* parameters $L, C = 1$, and assuming a transmission line of *unit length* ($l = 1$). The closed-loop transfer function is then

$$F(K) := \mathcal{F}_{\text{lower}}(G, -K) = \frac{K + \tanh s}{1 + K \tanh s}$$
$$= \frac{\sinh s + K \cosh s}{\cosh s + K \sinh s}. \tag{2.41}$$

There are an infinite number of closed-loop poles and zeros and if we restrict ourselves to *proportional* (also called *static*) controllers ($K \in \mathbb{R}$), these are

$$P = \left\{ s \in \mathbb{C} : s = -\text{artanh}\left(\frac{1}{K}\right) + \pi \jmath m, \ m \in \mathbb{Z}, \jmath = \sqrt{-1} \right\} \tag{2.42}$$

and

$$Z = \left\{ s \in \mathbb{C} : s = -\text{artanh}(K) + \pi \jmath m, \ m \in \mathbb{Z}, \jmath = \sqrt{-1} \right\}, \tag{2.43}$$

for which the plot of poles and zeros loci is in Fig. 2.7.

For $K = 0$, which corresponds to $R_{\text{L}} = \infty$, hence an open circuit on the load side, the closed-loop poles and zeros coincide with the open-loop ones, that is, they are located on the imaginary axis. For a short-circuit on the load side of the transmission line, which corresponds to $K = \infty$, the closed-loop poles and zeros are again on the imaginary axis.

It is exactly for the matching value of $K = 1$, that the closed-loop transfer function changes into

$$F = \frac{\sinh s + \cosh s}{\cosh s + \sinh s}$$
$$= \frac{\exp s}{\exp s}$$
$$= 1. \tag{2.44}$$

It has neither finite poles nor zeros, hence it is a constant function. Indeed, this is no cancellation of poles and zeros but rather simultaneous vanishing of poles and zeros. Thus, stability is trivially guaranteed.

We already know that $K_{\text{matched}} = 1$ achieves the reflection-free impedance matching but now will now examine how this controller K_{matched} relates to a stabilizing controller K_∞ that minimizes the $\mathcal{H}_\infty$ norm of the closed-loop transfer
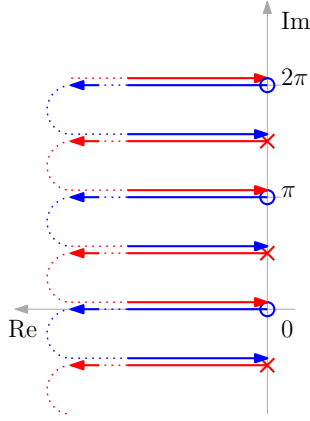
Figure 2.7: Root loci for the numerator (blue) and the denominator (red) of the closed-loop system—the lossless transmission line loaded with a real resistor with varying resistance. The closed-loop poles start at '×' and move to the left as R_{L} decreases (K increases). For the vanishing load resistance (infinite controller's gain) the closed-loop poles are back on the imaginary axis, this time in the positions '∘' of the open-loop zeros. Similarly, closed-loop zeros set out from '∘' to the left and after K crosses 1 they return to the positions of open-loop poles on the imaginary axis

function T, that is,

$$K_\infty = \underset{K \in \mathbb{R}_+}{\operatorname{argmin}} \left\| \frac{\sinh s + K \cosh s}{\cosh s + K \sinh s} \right\|_\infty. \tag{2.45}$$

Designing an $\mathcal{H}_\infty$-optimal controller for an infinite-dimensional system is a challenging task [21] because the system transfer function is irrational and one might anticipate that the optimal controller must be infinite-dimensional as well. However, a remarkable observation that we are going to prove is that if we restrict ourselves to proportional controllers, the minimum norm is achieved by the "matching controller", which is just a real-valued gain (a constant)! Namely,

$$K_\infty = K_{\mathrm{matched}} = 1. \tag{2.46}$$

Furthermore, from (2.40) we know that the matching controller makes the closed-loop transfer function identical to its own transfer function, hence

$$F_\infty = K_\infty, \tag{2.47}$$

which can be written explicitly as

$$K_\infty = \mathcal{F}_{\text{lower}}(G, -K). \tag{2.48}$$

Even though we are going to extend this results by considering dynamical controllers (including those with irrational transfer functions), the restriction of optimal control design to proportional controllers is surprising and interesting on its own, hence we state it as a lemma and prove it. And we will do it for the general nonnormalized lossless transmission line.

Lemma 1. *We consider the closed-loop transfer function $F(s) = Y_c \frac{K + Y_c \tanh(l\gamma(s))}{Y_c + K \tanh(l\gamma(s))}$, which corresponds to the admittance of a lossless transmission line with a characteristic admittance $Y_c = \sqrt{C/L}$, length l and the propagation function $\gamma(s) = \sqrt{LC}s$, terminated with a resistive load characterized with a real admittance K. A stabilizing "controller" (=load admittance) K_∞ that minimizes the $\mathcal{H}_\infty$ norm of the closed-loop transfer function F can be found as the positive solution of the quadratic (in K_∞) equation $K_\infty = Y_c \frac{K_\infty + Y_c \tanh(l\gamma(s))}{Y_c + K_\infty \tanh(l\gamma(s))}$. This solution is $K_\infty = Y_c = \left(\frac{C}{L}\right)^{\frac{1}{2}}$.*

Proof. First, in order to get some insight, let's restrict ourselves to the normalized line $(L, C = 1)$ of unit length $(l = 1)$. The proof boils down to verifying that $\|F\|_\infty^2 = \max\{K^2, \frac{1}{K^2}\}$. This can be seen by evaluating the squared magnitude frequency response

$$|F(\jmath\omega)|^2 = \overline{F(\jmath\omega)}\, F(\jmath\omega) \tag{2.49}$$

$$= \frac{K^2 + \tan^2(\omega)}{1 + K^2 \tan^2(\omega)} \tag{2.50}$$

$$= \frac{K^2 \cos^2(\omega) + \sin^2(\omega)}{\cos^2(\omega) + K^2 \sin^2(\omega)}, \tag{2.51}$$

which is periodic with the period of π and the local minima and maxima are located at integer multiples of $\pi/2$. The typical magnitude frequency responses of F (squared) are in Fig. 2.8 for $K = 0.9$, 1.1 and $K = 1.0$.

Now, consider the full case in which L, C and/or l are not necessarily of unit value. Then it can be shown that $|F(\jmath\omega)|^2$ is periodic with the period of $\frac{\pi}{l\sqrt{LC}}$ and the extrema are located at positions equal to integer multiples of $\frac{\pi}{2l\sqrt{LC}}$ and they assume values either K^2 or $\frac{Y_c^2}{K^2} = \frac{1}{K^2}\frac{C}{L}$. Thus the optimal setting for the positive and real-valued proportional controller is $K_\infty = Y_c = \left(\frac{C}{L}\right)^{\frac{1}{2}}$, which satisfies the quadratic equation.

$\square$
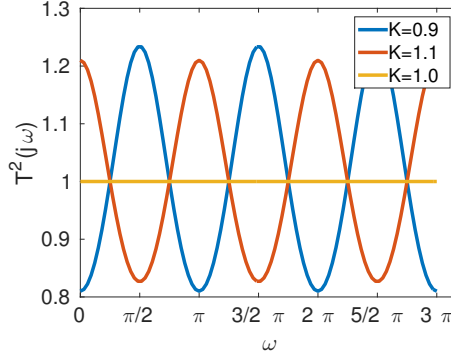
Figure 2.8: Magnitude frequency responses (squared) of the closed-loop transfer function F for three values of K

Although knowing that the proportional (static) controller that minimizes the $\mathcal{H}_\infty$ norm of the closed-loop transfer function can be computed without any resort to solving Riccati equations (or whatsoever), the question is, if any further performance improvement can be achieved by extending the search to dynamical controllers.

2.4 Dynamical $\mathcal{H}_\infty$-optimal control problem for a lossless transmission line

We have just learned that with a proportional controller we can beat $\|F\|_\infty$ as down as to $(C/L)^{\frac{1}{2}}$. For the normalized and unit-length transmission line this means we can achieve $\|F\|_\infty = 1$.

We will now show that there is a lower bound on the achievable $\mathcal{H}_\infty$ norm of the closed-loop transfer function F, that is

$$\|F\|_\infty \geq Y_{\mathrm{c}}, \tag{2.52}$$

which, again, for the normalized and unit-length transmission line specializes to

$$\|F\|_\infty \geq 1. \tag{2.53}$$

In order to prove the existence of this lower bound, we use the popular *scattering description*, which we recap next.

2.4.1 Scattering description

History of the concept

The idea of scattering description (or representation) of dynamical systems has its roots in research in fundamental physics in 1930s [83]. But soon it found its way into electrical engineering. Namely, it was simultaneously developed during the WWII in Belgium by Belevitch and in the USA by Dicke, Montgomery and Purcell. Belevitch presented his results in his dissertation in 1945 and reproduced them partially three years later in [8]). The results by Dicke and his colleagues were published at the same time [17], [51]. Whereas the former considered circuits composed of lumped elements, the latter focused on response of spatially distributed circuits in microwave frequency regions.

Later the concept was further developed by Kurokawa in his paper [38] and book [39]. In particular, he elaborates on distinction between different types of wave variables: voltage, current, power waves.

The concept of scattering description has found its way to perhaps every textbook on electrical circuits such as [37], [16], [13], [54], [1] and [5] and including Belevitch's own monograph [7]. Especially those focused on microwave frequencies such as [69] and transmission lines [49], [42]. Among shorter texts, [85] or [43] can be recommended.

Scattering description

Scattering description is based on one particular transformation of the original "physical variables" u and i into a new pair of variables

$$\hat{u}^+ = \frac{1}{2}(\hat{u} + Z_{\text{ref}}\,\hat{i}), \tag{2.54}$$

$$\hat{u}^- = \frac{1}{2}(\hat{u} - Z_{\text{ref}}\,\hat{i}), \tag{2.55}$$

where Z_{ref} is some *reference impedance* that parameterizes the transformation and the variables u^+ and u^- are called *wave variables* for the reasons to be cleared up briefly. Ignore for the moment the fact that we have already discussed objects with identical symbols (u^+ and u^-) earlier in the paper in (2.10); (indeed, they are related). The two new variables have the physical dimension of voltage. Although we can similarly transform the current, we will stick with the voltage.

We will write (2.54) and (2.55) in the matrix-vector format

$$\begin{bmatrix} \hat{u}^+ \\ \hat{u}^- \end{bmatrix} = \frac{1}{2} \begin{bmatrix} 1 & Z_{\text{ref}} \\ 1 & -Z_{\text{ref}} \end{bmatrix} \begin{bmatrix} \hat{u} \\ \hat{i} \end{bmatrix}. \tag{2.56}$$

Inverting this relationship we get

$$\begin{bmatrix} \hat{u} \\ \hat{i} \end{bmatrix} = \begin{bmatrix} 1 & 1 \\ Z_{\text{ref}}^{-1} & -Z_{\text{ref}}^{-1} \end{bmatrix} \begin{bmatrix} \hat{u}^+ \\ \hat{u}^- \end{bmatrix}, \tag{2.57}$$

wherein we label the matrix on the right-hand side as T, that is

$$T = \begin{bmatrix} 1 & 1 \\ Z_{\text{ref}}^{-1} & -Z_{\text{ref}}^{-1} \end{bmatrix}. \tag{2.58}$$

Compare this with (2.10) and (2.11) combined with (2.13)—the scattering framework formalizes (and generalizes) the split of the original physical variables into incident and reflected quantities (waves). Note that here we consider some as of yet unspecified reference impedance Z_{ref}.

An important step in our analysis is to apply Laplace transform to the temporal variable in (2.7), which turns the two PDEs into a set of two ODEs in a state-space format (note that the independent variable is x and the matrix A is parameterized by s)[1]

$$\begin{bmatrix} \frac{\partial \hat{u}(x,s)}{\partial x} \\ \frac{\partial \hat{i}(x,s)}{\partial x} \end{bmatrix} = \underbrace{\begin{bmatrix} 0 & -Ls \\ -Cs & 0 \end{bmatrix}}_{A(s)} \begin{bmatrix} \hat{u}(x,s) \\ \hat{i}(x,s) \end{bmatrix}. \tag{2.59}$$

Standard procedure in the analysis of state space models is to diagonalize the system's A matrix through an eigen-decomposition

$$\begin{bmatrix} \frac{\partial \hat{u}}{\partial x} \\ \frac{\partial \hat{i}}{\partial x} \end{bmatrix} = \begin{bmatrix} 1 & 1 \\ Z_{\text{c}}^{-1} & -Z_{\text{c}}^{-1} \end{bmatrix} \begin{bmatrix} -\gamma & 0 \\ 0 & \gamma \end{bmatrix} \begin{bmatrix} 1 & 1 \\ Z_{\text{c}}^{-1} & -Z_{\text{c}}^{-1} \end{bmatrix}^{-1} \begin{bmatrix} \hat{u} \\ \hat{i} \end{bmatrix}, \tag{2.60}$$

where the eigenvalues are given in terms of

$$\gamma(s) = \sqrt{LC}s. \tag{2.61}$$

The middle term in the decomposition captures the decoupled dynamics in the new wave variables

$$\begin{bmatrix} \frac{\partial \hat{u}^+(x,s)}{\partial x} \\ \frac{\partial \hat{u}^-(x,s)}{\partial x} \end{bmatrix} = \begin{bmatrix} -\gamma(s) & 0 \\ 0 & \gamma(s) \end{bmatrix} \begin{bmatrix} \hat{u}^+(x,s) \\ \hat{u}^-(x,s) \end{bmatrix} \tag{2.62}$$

Obviously, the transformation given by (2.54) and (2.55) diagonalizes the state-space system for the particular choice

$$Z_{\text{ref}} = Z_{\text{c}}. \tag{2.63}$$

---

[1]Note that by transforming the temporal variable, we follow a completely different path here then what is promoted in [6], where they turn the PDE into a state-space model by Fourier-transforming the spatial variable.
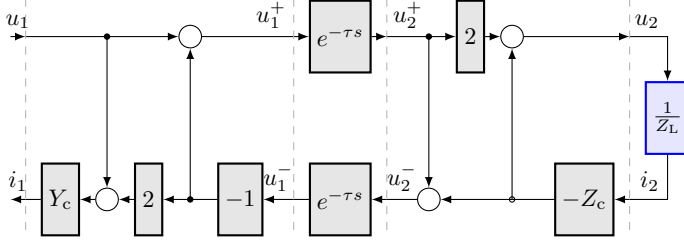
Figure 2.9: Diagonal decomposition of the original two-port network description

The reason why we struggled to obtain a diagonal model is that now we can easily solve it independently for each state variable (note that the independent variable is x here)

$$\hat{u}^+(x,s) = e^{-\gamma(s)x}\,\hat{u}^+(0,s) \tag{2.64}$$

$$\hat{u}^-(x,s) = e^{\gamma(s)(x-l)}\,\hat{u}^-(l,s) = e^{-\gamma(s)(l-x)}\,\hat{u}^-(l,s), \tag{2.65}$$

which allows us to find transfer functions

$$\frac{\hat{u}_2^+(s)}{\hat{u}_1^+(s)} = e^{-\gamma(s)\,l}, \tag{2.66}$$

$$\frac{\hat{u}_1^-(s)}{\hat{u}_2^-(s)} = e^{-\gamma(s)\,l}, \tag{2.67}$$

where

$$\gamma(s)l = \sqrt{LC}ls = \frac{l}{c}s = \tau s \tag{2.68}$$

and τ is the time the wave needs to travel across the transmission line of the length l at velocity c.

This decomposition can also be visualized in the block diagram in Fig. 2.9, wherein we used

$$\begin{bmatrix} \hat{i}_1 \\ \hat{u}_1^+ \end{bmatrix} = \begin{bmatrix} Y_c & -2Y_c \\ 1 & -1 \end{bmatrix} \begin{bmatrix} \hat{u}_1 \\ \hat{u}_1^- \end{bmatrix} \tag{2.69}$$

and

$$\begin{bmatrix} \hat{u}_2 \\ \hat{u}_2^- \end{bmatrix} = \begin{bmatrix} -Z_c & 2 \\ -Z_c & 1 \end{bmatrix} \begin{bmatrix} \hat{i}_2 \\ \hat{u}_2^+ \end{bmatrix}. \tag{2.70}$$

The transfer function from u_1^+ to u_1^- can be written as

$$\frac{\hat{u}_1^-(s)}{\hat{u}_1^+(s)} = \frac{\hat{u}_1^-(s)}{\hat{u}_2^-(s)}\frac{\hat{u}_2^-(s)}{\hat{u}_2^+(s)}\frac{\hat{u}_2^+(s)}{\hat{u}_1^+(s)}, \tag{2.71}$$

in which we label the middle transfer function as $S_{\mathrm{L}}(s)$

$$S_{\mathrm{L}}(s) := \frac{\hat{u}_2^-(s)}{\hat{u}_2^+(s)}, \tag{2.72}$$

and it can be found either directly from the block diagram or by substituting for the $\hat{u}_2^+$ and $\hat{u}_2^-$ the original (physical) variables $\hat{u}_2$ and $\hat{i}_2$ and relating the two physical variables by their known relationship on the load side of the line

$$\hat{u}_2(s) = Z_{\mathrm{L}}(s)\,\hat{i}_2(s). \tag{2.73}$$

Then substituting this into (2.54) and (2.55) while invoking (2.63) yields

$$\hat{u}_2^+(s) = (Z_{\mathrm{L}}(s) + Z_{\mathrm{c}}(s))\,\hat{i}(l, s), \tag{2.74}$$

$$\hat{u}_2^-(s) = (Z_{\mathrm{L}}(s) - Z_{\mathrm{c}}(s))\,\hat{i}(l, s), \tag{2.75}$$

which finally gives the desired third transfer function

$$S_{\mathrm{L}}(s) = \frac{Z_{\mathrm{L}}(s) - Z_{\mathrm{c}}(s)}{Z_{\mathrm{L}}(s) + Z_{\mathrm{c}}(s)}. \tag{2.76}$$

Within the microwave engineering community this transfer function has its name—the *reflection coefficient* or *reflectance*[2]. Making it zero by setting

$$Z_{\mathrm{L}} = Z_{\mathrm{c}} \tag{2.77}$$

is how the impedance matching condition (2.12) was arrived at.

For completeness we state here that in general the relationship between the incident and reflected waves on both ports is captured by means of *scattering matrix S*

$$\begin{bmatrix} \hat{u}_1^- \\ \hat{u}_2^- \end{bmatrix} = \begin{bmatrix} S_{11}(s) & S_{12}(s) \\ S_{21}(s) & S_{22}(s) \end{bmatrix} \begin{bmatrix} \hat{u}_1^+ \\ \hat{u}_2^+ \end{bmatrix} \tag{2.78}$$

used widely in the circuits [7],[54],[37] and microwave communities [69]. Scattering matrix is nothing else then a two-port version of the reflection coefficient defined in (2.72) for a one-port—the scattering matrix relates the incident waves (u_1^+ and u_2^+) with the reflected waves (u_1^- and u_2^-). For the reference impedance set equal to the characteristic impedance of the line, the diagonal entries of the scattering matrix vanish

$$S(s) = \begin{bmatrix} 0 & e^{-\tau s} \\ e^{-\tau s} & 0 \end{bmatrix} \tag{2.79}$$

and (2.71) can be evaluated as $\mathcal{F}_{\mathrm{lower}}(S, S_{\mathrm{L}})$ into

$$\frac{\hat{u}_1^-(s)}{\hat{u}_1^+(s)} = e^{-2\tau s} S_{\mathrm{L}}(s). \tag{2.80}$$

---

[2]A more common symbol for the reflectance in the literature is Γ but here we choose S_{L} to emphasize that it is just a scalar version of the scattering matrix S.

2.4.2 Closed-loop transfer function parameterized by the reflection coefficient

At the end of the day, what we are after is the closed-loop transfer function $F(s) = \hat{i}_1(s)/\hat{u}_1(s)$ relating the physical variables u_1 and i_1. It can be written using the wave variables as

$$
\begin{aligned}
F(s) &= \frac{\hat{i}_1(s)}{\hat{u}_1(s)} \\
&= \frac{\hat{i}_1^+(s) - \hat{i}_1^-(s)}{\hat{u}_1^+(s) + \hat{u}_1^-(s)} \\
&= \frac{1}{Z_{\text{ref}}(s)} \frac{\hat{u}_1^+(s) - \hat{u}_1^-(s)}{\hat{u}_1^+(s) + \hat{u}_1^-(s)},
\end{aligned}
\tag{2.81}
$$

which for $Z_{\text{ref}} = Z_{\text{c}}$ gives

$$
\begin{aligned}
F(s) &= \frac{1}{Z_{\text{c}}} \frac{\hat{u}_1^+(s) \left(1 - e^{-2\tau s} S_{\text{L}}(s)\right)}{\hat{u}_1^+(s) \left(1 + e^{-2\tau s} S_{\text{L}}(s)\right)} \\
&= \frac{1}{Z_{\text{c}}} \frac{1 - e^{-2\tau s} S_{\text{L}}(s)}{1 + e^{-2\tau s} S_{\text{L}}(s)}.
\end{aligned}
\tag{2.82}
$$

For convenience (and without loss of generality), we will again consider the normalized case and unit-length case, for which $Z_{\text{c}} = 1$, $\tau = 1$ and

$$
F(s) = \frac{1 - e^{-2s} S_{\text{L}}(s)}{1 + e^{-2s} S_{\text{L}}(s)}.
\tag{2.83}
$$

Voilà a new parameterization of achievable closed-loop transfer functions!

Can we beat the $\mathcal{H}_\infty$ norm of F in (2.83) below 1? Choosing the reflection coefficient $S_{\text{L}}(s) = e^{2s}$ sets the closed-loop transfer function to zero

$$
F(s) = \frac{1 - e^{-2s} e^{2s}}{1 + e^{-2s} e^{2s}} = 0/2 = 0.
\tag{2.84}
$$

An important observation is that this reflection coefficient S_{L} is not *proper* (it is the opposite of a delay). This trivial fact can also be seen formally from unboundedness of $S_{\text{L}}(s)$ in the extended right half plane (see [15]). Although one may feel that there is no need to require properness (hence realizability) of the reflectance $S_{\text{L}}(s)$ because what we are only interested in is realizability of the "controller" $K(s)$ in the physical domain, the need for properness of S_{L} can be physically justified as well. Being nonproper means that if a voltage is applied at the input port, the reaction of the controller on the load side (the reflected wave)

can be delivered to the input port before the incident wave hits the controller port. In this particular case, the controller essentially decouples the output i_1 from the input u_1: although voltage is applied to the input terminal pair of a long transmission line, no current flows from the generator to the line.

Making a physical analogy with a slender flexible bar vibrating in a longitudinal direction, the force acting on one end of the bar will see no movement as a response because the controller on the other end of the bar sends special waves with anticipation of the force so that the end of the bar on which the force is exerted will behave as a "wall", fixed in the inertial space. This is not realizable.

But we can also analyze the resulting controller itself. We can get the transfer function by transforming S_{L} back to the load impedance using

$$Z_{\mathrm{L}} = \frac{1 + S_{\mathrm{L}}}{1 - S_{\mathrm{L}}}, \tag{2.85}$$

from which the corresponding "controller" (admittance) is

$$K(s) = \frac{1}{Z_{\mathrm{L}}(s)} = \frac{1 - e^{2s}}{1 + e^{2s}}. \tag{2.86}$$

In the time-domain, the relationship between the input and output of the controller is (note that here we use the variables as in Fig. 2.1)

$$u(t) + u(t + 2) = y(t) - y(t + 2), \tag{2.87}$$

that is,

$$u(t) = -u(t + 2) + y(t) - y(t + 2). \tag{2.88}$$

Here comes the key argument that it is not possible to get the norm of the closed-loop system under 1. The transfer function F in (2.83) can be factored as

$$F(s) = 1 - 2\frac{e^{-2s} S_{\mathrm{L}}(s)}{1 + e^{-2s} S_{\mathrm{L}}(s)}. \tag{2.89}$$

Match this to Fig. 2.9. The first term on the right (the scalar 1) corresponds to the leftmost direct path from u_1 to i_1 (in the nonnormalized case this path contains the Z_{c} term) and everything else in the diagram comes from the reflection of the wave (this also nicely reinforces the definition of the characteristic impedance Z_{c} as the *local* characteristic). Now, in order to get

$$\|F\|_\infty < 1, \tag{2.90}$$

we must have

$$\left| 1 - 2\frac{e^{-2\jmath\omega} S_{\mathrm{L}}(\jmath\omega)}{1 + e^{-2\jmath\omega} S_{\mathrm{L}}(\jmath\omega)} \right| < 1, \qquad \forall \omega \in \mathbb{R}. \tag{2.91}$$

Let's label the second term as

$$H(\jmath\omega) = 2\frac{e^{-2\jmath\omega}\, S_\mathrm{L}(\jmath\omega)}{1 + e^{-2\jmath\omega}\, S_\mathrm{L}(\jmath\omega)}, \tag{2.92}$$

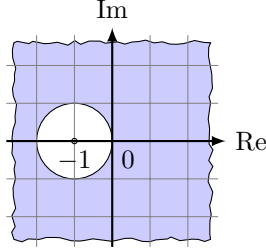and it must reside for all frequencies in the open unit circle centered at 1, see Fig. 2.10.

Figure 2.10: A unit circle centered at -1 inside which the Nyquist curve $H(\jmath\omega) = 2\frac{e^{-2\jmath\omega}\, S_\mathrm{L}(\jmath\omega)}{1+e^{-2\jmath\omega}\, S_\mathrm{L}(\jmath\omega)}$ must reside, should the norm of the closed-loop transfer function be strictly smaller than 1

If $S_\mathrm{L}(s)$ is *strictly proper*, then $\lim_{s\to\infty} H(s) = 0$, which breaks (2.91). If $S_\mathrm{L}(s)$ is just *proper* (see [15] for a discussion of properness for irrational transfer functions), the limit need not exist but at least the function must be bounded as the frequency ω goes to infinity along the imaginary axis. Therefore

$$\limsup_{\omega\to\infty} \left| 2\frac{S_\mathrm{L}(\jmath\omega)}{1 + e^{-2\jmath\omega}\, S_\mathrm{L}(\jmath\omega)} \right| < \infty \tag{2.93}$$

and with a suitable choice of S_L one can fit the above term into the circle. But then comes the delay term, which effectively rotates the content of the term above around the origin of the complex plane—no way to stick to the inside of the circle in Fig. 2.10 after such rotation.

To conclude, even dynamical controllers can not make the $\mathcal{H}_\infty$ norm of the closed-loop transfer function F strictly smaller than 1. And since we have already found one controller that achieves the norm exactly 1, we can claim we have found an optimal controller. We do not exclude the possibility that there are dynamical controllers that are optimal too. But we are happy with a simple one—a proportional one. We conclude by stating the result as a theorem

Theorem 1. *The achievable $\mathcal{H}_\infty$ norm of the closed-loop transfer function $F = \mathcal{F}_\mathrm{lower}(G, K)$, where G is the 2×2 matrix transfer function corresponding to the*

inverse hybrid model of a normalized lossless transmission line and K corresponding to the admittance of the load, is bounded from below by Y_c. Moreover, this lower bound can be achieved using a proportional controller corresponding to a matching real admittance.

Proof. The lower-boundedness by 1 was proved for the normalized and unit-length case in the text above. The existence of the proportional controller achieving the value of the lower bound is given by the Lemma. □

2.4.3 Power waves

To gain some additional insight into the difficulties of extending this result, it is worth mentioning that the transformation given by (2.54) and (2.55) is not the only reasonable one. Another useful one is

$$\hat{a} = \frac{1}{2} \frac{\hat{u} + Z_{\text{ref}}\,\hat{i}}{\sqrt{\Re(Z_{\text{ref}})}}, \tag{2.94}$$

$$\hat{b} = \frac{1}{2} \frac{\hat{u} - Z_{\text{ref}}\,\hat{i}}{\sqrt{\Re(Z_{\text{ref}})}}, \tag{2.95}$$

which for a real impedance $Z_{\text{ref}} = R_{\text{ref}}$ simplifies to

$$a = \frac{1}{2} \frac{u + R_{\text{ref}}\,i}{\sqrt{R_{\text{ref}}}}, \tag{2.96}$$

$$b = \frac{1}{2} \frac{u - R_{\text{ref}}\,i}{\sqrt{R_{\text{ref}}}}. \tag{2.97}$$

Sticking for a while with real reference impedances, the new variables a and b are called *power waves*. The reason for this terminology is that if we now square the two variables, we get

$$a^2 = \frac{1}{4} \frac{(R_{\text{L}} + R_{\text{ref}})^2}{R_{\text{ref}}} i^2, \tag{2.98}$$

$$b^2 = \frac{1}{4} \frac{(R_{\text{L}} - R_{\text{ref}})^2}{R_{\text{ref}}} i^2, \tag{2.99}$$

which simplifies significantly if $R_{\text{L}} = R_{\text{ref}}$

$$a^2 = R_{\text{ref}}\,i^2, \tag{2.100}$$

$$b^2 = 0. \tag{2.101}$$

With the interpretation of R_{ref} as the internal resistance of some generator of voltage e that feeds the load, the above condition corresponds to the maximum power transfer condition (2.16). To see this, plug in the current given by

$$i = \frac{e}{2R_{\mathrm{ref}}}, \tag{2.102}$$

into (2.100) to get

$$a^2 = \frac{e^2}{4R_{\mathrm{ref}}}, \tag{2.103}$$

which should look familiar since for $R_{\mathrm{ref}} = R_{\mathrm{G}}$ this agrees with the *available power* (2.18), whereas the squared b variable is the extra power that is dissipated on the internal resistor (in addition to the minimum power that needs to be burnt there anyway). If the load is not matched, the power delivered to the load can be written as

$$\mathcal{P}(t) = a^2(t) - b^2(t), \tag{2.104}$$

hence the name *power waves*—if not all the available power is used by the load, we view as if the power wave was reflected on the load and sent back to the generator.

The situation gets more complicated when *complex reference impedance* is used. As proposed (among others) by [38], the transformation can be defined differently

$$\hat{a} = \frac{1}{2} \frac{\hat{u} + Z_{\mathrm{ref}}\,\hat{i}}{\sqrt{\Re(Z_{\mathrm{ref}})}}, \tag{2.105}$$

$$\hat{b} = \frac{1}{2} \frac{\hat{u} - Z^*_{\mathrm{ref}}\,\hat{i}}{\sqrt{\Re(Z_{\mathrm{ref}})}}. \tag{2.106}$$

One can check (or see in [70]) that for a complex reference impedance (hence load and internal impedance), (2.104) is only valid with this modified transformation[3]. The original voltage or current waves (possibly normalized by a real constant) cannot be immediately related to power waves.

Although introduced a long time ago, there are still some disputes such as [84] related to this transformation. Furthermore, note that the concept of power waves is still related to the harmonic generators. The transformation will have to be further modified by replacing the harmonic conjugates with paraconjugates

---

[3]Beware the issue of time- vs. frequency-domain signal. Once switching to frequency domain (Fourier transform), evaluating a power can be quite tricky. Some newer textbooks even have it wrong in that they define power as a product of Laplace transformed current and voltage. But this restricts the signals to decaying ones (unless one brings in the distribution theory...), and then, what Parseval theorem gives, is a relationship for total energies and not power, not to speak of average power. The classical books on electric networks and circuits compute the average power in a harmonic steady state using using phasors.

(see [37], page 291). We will not delve into these since in this work we assume a lossless transmission line, hence the characteristic resistance will be real. Our motivation for including this material was to highlight the possible complications when considering lossy transmission lines, for which the characteristic impedance is complex.

2.5 Conclusions and future research

In this work we proved that the impedance matching load for a lossless transmission line minimizes the $\mathcal{H}_\infty$ norm of the admittance of the loaded transmission line. This result can be appealing for at least two reasons: first, this gives an benchmark example for computational design of $\mathcal{H}_\infty$-optimal controller for an infinite-dimensional linear dynamical system described by an irrational transfer function. Second, this result may help develop some insight into scaling of chains of interconnected lumped dynamical systems. Research in this direction is under way.

The restriction to lossless transmission lines that we applied in this work turns out crucial. It is only in the lossless case that the characteristic impedance of a transmission line is just a positive real constant. The characteristic impedance of a lossy line is irrational transfer function. Moreover, the distinction between the reflection-free impedance matching and conjugate impedance matching starts playing a role, which deserves to be investigated further. In particular, it looks worthy to investigate the possibilities in casting the problem of maximum power transfer in the general *Integral Quadratic Constraints (IQC)* framework [47].

3 Spatially discrete medium—chains of lumped systems

3.1 Formats of models of a two-port linear network

Thanks to Maxwell analogy among physical domains (see, for example, [9]), we can identify the same structure of dynamical systems across several physical domains. The structure of interest for us is also shared by *ladders* or cascades of simple sections composed of basic electric elements as shown in Fig. 1.4. Without loss of generality we will adhere to the electric domain for a while and discuss physical analogies later.

3.1.1 Two-port networks

Let us recall the concept of a *two-port network* here. This is a dynamical system which interacts with the environment (other systems) by exchanging power through two *ports*. Each port is realized as a pair of *terminals* (wires, leads). The port voltage is defined as a potential difference the two terminals. The port current enters one terminal and leaves through the other, see Fig. 3.1
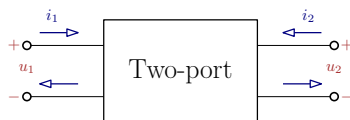

Figure 3.1: Electric two-port network. The port 1 is characterized by the voltage u_1 and the current i_1, the port 2 is similarly characterized by u_2 and i_2

A popular (because fairly general) internal structure of a two-port network is in Fig. 3.2.

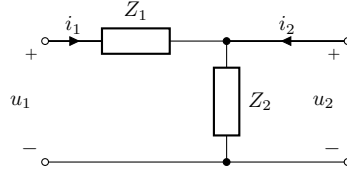In this work we will restrict ourselves to L-sections in which the impedances

Figure 3.2: An L-section with a series and shunt impedances, $Z_1(s)$ and $Z_2(s)$, respectively

that define the section are frequency-dependent and their Laplace transforms are

$$Z_1(s) = Ls + R, \tag{3.1}$$
$$Z_2(s) = 1/Y_2(s) \tag{3.2}$$
$$Y_2(s) = Cs + G. \tag{3.3}$$
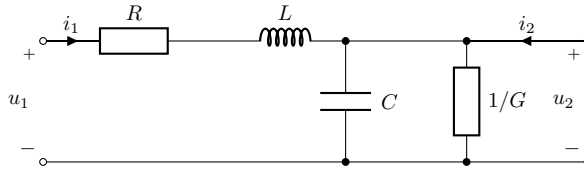
as in Fig. 3.3.

Figure 3.3: A single lumped L-section from which the resulting chain is composed

We will actually consider lossless section, that is, $R = 0$ and $G = 0$, in this paper.

In order to uniquely describe the system, two of these four variables u_1, i_1, u_2, i_2 must be chosen as the *inputs* and the other two are then the *outputs*. This gives rise to several formats of *input-output models*. Here we will recall just two of them: *hybrid* model (or actually *inverse hybrid*) and *cascade* (also called *chain* or *transmission* or *ABCD* model), or actually its inverse (or backward) version.

3.1.2 Inverse hybrid transfer function matrix

Let us start with the *inverse hybrid* model, which is driven by u_1 and i_2 (we call them *inputs*) and whose response is i_1 and u_2 (we call them *outputs*) as in Fig. 3.5. The entries of the corresponding 2×2 transfer function matrix are called *g-parameters*. Note that the *hybrid* description without the adjective *inverse* is commonly defined with i_1 and u_2 as the inputs and u_1 and i_2 as the outputs.

The entries of the corresponding 2×2 matrix are then the popular *h-parameters*. The inverse hybrid transfer function model is

$$\begin{bmatrix} \hat{i}_1(s) \\ \hat{u}_2(s) \end{bmatrix} = \begin{bmatrix} g_{11}(s) & g_{12}(s) \\ g_{21}(s) & g_{22}(s) \end{bmatrix} \begin{bmatrix} \hat{u}_1(s) \\ \hat{i}_2(s) \end{bmatrix}. \tag{3.4}$$

In our case of an L-section with a series impedance $Z_1(s)$ and a shunt admittance $Y_2(s)$ the inverse hybrid description is

$$\begin{bmatrix} \hat{i}_1(s) \\ \hat{u}_2(s) \end{bmatrix} = \underbrace{\begin{bmatrix} \frac{Y_2(s)}{1+Z_1(s)Y_2(s)} & -\frac{1}{1+Z_1(s)Y_2(s)} \\ \frac{1}{1+Z_1(s)Y_2(s)} & \frac{Z_1(s)}{1+Z_1(s)Y_2(s)} \end{bmatrix}}_{G(s)} \begin{bmatrix} \hat{u}_1(s) \\ \hat{i}_2(s). \end{bmatrix}. \tag{3.5}$$

Considering the lossless and normalized case, that is, if $R = G = 0$[1] and $L = C = 1$, the inverse hybrid description is

$$\begin{bmatrix} \hat{i}_1(s) \\ \hat{u}_2(s) \end{bmatrix} = \begin{bmatrix} \frac{s}{1+s^2} & -\frac{1}{1+s^2} \\ \frac{1}{1+s^2} & \frac{s}{1+s^2} \end{bmatrix} \begin{bmatrix} \hat{u}_1(s) \\ \hat{i}_2(s). \end{bmatrix}. \tag{3.6}$$

This format of a model is particularly useful when a one-port load is to be attached to a given two-port network as in Fig. 3.4.
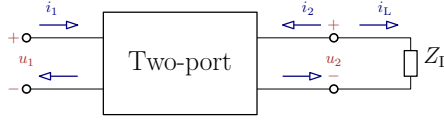

Figure 3.4: Two-port loaded on the port 2 with an impedance Z_L.

The convenience can be found in the signal-flow graph in Fig. 3.5—depending on the chosen causality (whether the voltage u_1 or the current i_1 are the inputs) we can immediately substitute one of the two equations for the load

$$-\hat{i}_2(s) = \hat{i}_\mathrm{L}(s) = Y_\mathrm{L}(s)\hat{u}_2(s) \tag{3.7}$$

or

$$\hat{u}_2(s) = Z_\mathrm{L}(s)\hat{i}_\mathrm{L}(s) = -Z_\mathrm{L}(s)\hat{i}_2(s) \tag{3.8}$$

into (3.4) to get a transfer function from u_1 to i_1, see the discussion of *linear fractional transformation* in the next section.

---

[1]Beware that there is a notational clash between the usage of G for the inverse hybrid matrix and the shunt conductance. We do not resolve it by introducing some less common symbols for one of the two variables. The context will certainly help resolve avoid confusion.
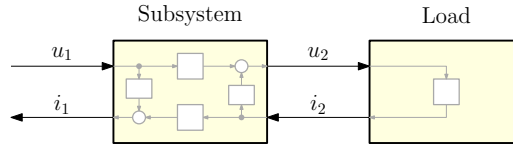
Figure 3.5: Signal flow graph for an interconnection of two two-ports which are modeled using the (inverse) hybrid parameters

3.1.3 Inverse chain transfer function matrix

The other format of a mathematical model of a two-port network that we are going to use is the *inverse chain* (also called *inverse ABCD*) transfer function matrix. The matrix defines the input-output model (after applying Laplace transform)

$$\begin{bmatrix} \hat{u}_2(s) \\ -\hat{i}_2(s) \end{bmatrix} = \begin{bmatrix} b_{11}(s) & b_{12}(s) \\ b_{21}(s) & b_{22}(s) \end{bmatrix} \begin{bmatrix} \hat{u}_1(s) \\ \hat{i}_1(s) \end{bmatrix}. \tag{3.9}$$

Note the minus sign with the output current i_2; the reason for its introduction is that this format then allows building the models of cascade interconnections as in Fig. 3.6 very easily—by multiplication of the inverse chain matrices (or by raising them to an integer power in the case of identical inverse chain matrices).

$$\begin{bmatrix} \hat{u}_2(s) \\ -\hat{i}_2(s) \end{bmatrix} = B_2 \begin{bmatrix} \hat{u}_1(s) \\ \hat{i}_1(s) \end{bmatrix} \tag{3.10}$$

$$= B_2 B_1 \begin{bmatrix} \hat{u}_0(s) \\ \hat{i}_0(s) \end{bmatrix}. \tag{3.11}$$
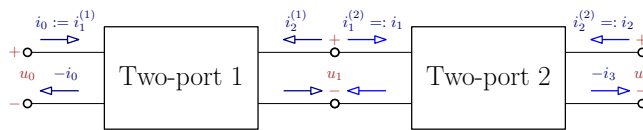

Figure 3.6: Chain (or cascade) interconnection of two two-ports.

For an L-section with a series impedance Z_1 and a shunt admittance Y_2, the inverse chain model is

$$\begin{bmatrix} \hat{u}_2(s) \\ -\hat{i}_2(s) \end{bmatrix} = \underbrace{\begin{bmatrix} 1 & -Z_1(s) \\ -Y_2(s) & 1 + Z_1(s)Y_2(s) \end{bmatrix}}_{B(s)} \begin{bmatrix} \hat{u}_1(s) \\ \hat{i}_1(s) \end{bmatrix}. \tag{3.12}$$

For the lossless and normalized case, that is, if $R = G = 0$ and $L = C = 1$, the (inverse) chain model is

$$\begin{bmatrix} \hat{u}_2(s) \\ -\hat{i}_2(s) \end{bmatrix} = \begin{bmatrix} 1 & -s \\ -s & 1+s^2 \end{bmatrix} \begin{bmatrix} \hat{u}_1(s) \\ \hat{i}_1(s) \end{bmatrix}, \tag{3.13}$$

Although in Fig. 3.7 we give a signal flow graph for this interconnection, note that there is a caveat when trying to give it the usual input-output interpretation because the two variables on a given port are not independent—they are coupled through the boundary conditions. Anyhow, we use the signal flow graph to encode graphically the structure of the corresponding equations.

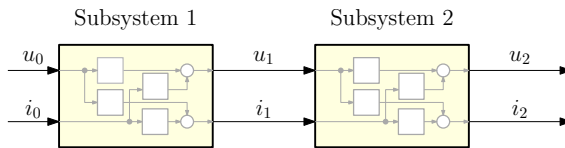Subsystem 1   Subsystem 2

Figure 3.7: Chain interconnection of two two-port networks described by their (inverse) *chain* transfer functions.

There is a relationship between the inverse chain matrix (the B transfer matrix above) and the inverse hybrid matrix (the G matrix above):

$$\begin{bmatrix} g_{11} & g_{12} \\ g_{21} & g_{22} \end{bmatrix} = \begin{bmatrix} -b_{22}^{-1}\,b_{21} & -b_{22}^{-1} \\ b_{11} - b_{12}\,b_{22}^{-1}\,b_{21} & -b_{12}\,b_{22}^{-1} \end{bmatrix}. \tag{3.14}$$

Beware that if we were to stick to the sign conventions for the B matrix (3.9) related to the current through the right port, the current i_2 in Fig. 3.7 is regarded as flowing into the port through the + terminal. This is unfortunately in conflict with the convention in our later Section 3.4.

3.2 Linear fractional transformation and feedback interconnection of two- and one-port networks

The feedback controller that we want to design (see Fig. 1.10) can be interpreted as a design of a suitable termination for a ladder network. In Fig. 3.8 we redraw such terminated ladder composed of several L-sections, each characterized by the (identical) inverse hybrid transfer function G, in a signal flow graph corresponding to the so-called *linear fractional transformation (LFT)* framework popular in control theory.

Note that from now on we change the indexing and start with 0 for the first voltage-current pair so that for n blocks (sections in the ladder) the voltage-current pair on the load side is indexed n.

Furthermore, because of our insistence on keeping the conventional directions of currents i_1 and i_2 (inside the two-port network through the corresponding + terminal), we deviate from the common control theory convention (for LFT) and consider a negative feedback here.
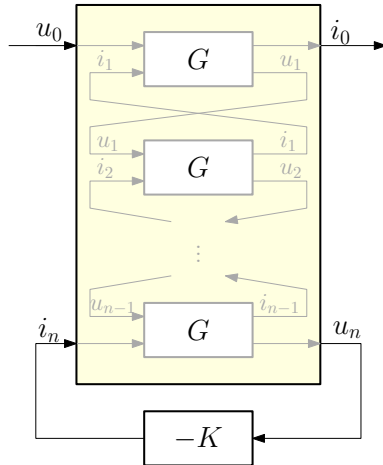

Figure 3.8: Lower linear fractional transformation of a generalized plant (grayed) with respect to the controller (with a transfer function $-K$). The plant is formed by interconnection of n blocks, each described by a transfer function matrix G

The closed-loop transfer function F from the *exogenous input* (u_0 in this case) to the *regulated output* (i_0 in this case) is given by

$$F = \mathcal{F}_{\text{lower}}(\tilde{G}, -K) \tag{3.15}$$

$$= \tilde{g}_{11} - \frac{\tilde{g}_{12} K \tilde{g}_{21}}{1 + \tilde{g}_{22} K}, \tag{3.16}$$

where $\tilde{G}$ is the inverse hybrid transfer function matrix for the ladder. Computing the inverse hybrid matrix transfer function of the whole chain (unterminated chain, the gray block in Fig. 3.8) can be quite tedious when using the inverse hybrid matrices G for the individual blocks—it is described by the *Redheffer star product* (see, for example, [87], Sec. 10.4). But it is easy when using the *(inverse) chain matrices B* for the individual blocks—the model is then obtained

as an integer power of B. This is what we exploit later. But first we state the goal of this paper.

3.3 $\mathcal{H}_\infty$ control of a chain (ladder) through a boundary subsystem

With the setup described in Fig. 3.8, the control design can be cast as an optimization problem: find the feedback controller K that not only stabilizes the feedback loop but also makes the transfer function from exogenous signals to the output regulated signals optimal *in some sense*.

One popular optimization framework is that of minimizing the $\mathcal{H}_\infty$ norm of the closed-loop system, that is,

$$\text{minimize} \left\| \mathcal{F}_{\text{lower}}(\tilde{G}, -K) \right\|_\infty, \tag{3.17}$$

over K stabilizing. Stabilization means that the closed-loop transfer function F resides in the space $\mathcal{H}_\infty$ of functions that are analytic and bounded in the (extended) complex right half-plane. The $\mathcal{H}_\infty$ norm of a scalar transfer function $F(s)$ is defined as

$$\|F\|_\infty = \sup_{\omega \in \mathbb{R}} |F(j\omega)|. \tag{3.18}$$

This norm also serves as the worst-case gain for the 2-norms of the corresponding time-domain input and output signals

$$\|F\|_\infty = \sup_{u \backslash \{0\}} \frac{\|i\|_2}{\|u\|_2}. \tag{3.19}$$

The physical interpretation for electrical ladders is that the peaks in the magnitude frequency response of the input-side admittance are minimized. By casting the controller design problem as the $\mathcal{H}_\infty$ optimization, we aim at reducing the oscillations of the current on the first section (closest to the input) in response to the change in the applied (input) voltage as much as possible. Obviously, the oscillations are induced by the interaction with the other sections in the ladder. Our controller aims at mitigating these interconnection effects.

We will also study how the achievable performance scales with the length of the ladder (the chain).

3.4 Diagonalization of the chain model and reflectionless impedance matching

When analyzing a given chain, we need to build its overall model, be it the over-all *inverse hybrid* transfer function matrix or *backward chain* transfer function matrix (or any other format), and then analyze the properties of these result-ing transfer function matrices (often of very high order). There is another path, though. Recalling that the chain matrix B relates the voltage-current pairs at two neighboring sections (indexed with an integer k), we can think of some fictitious discrete dynamical system described by the equation

$$\begin{bmatrix} \hat{u}_{k+1}(s) \\ \hat{i}_{k+1}(s) \end{bmatrix} = \underbrace{\begin{bmatrix} 1 & -Z_1(s) \\ -Y_2(s) & 1 + Z_1(s)Y_2(s) \end{bmatrix}}_{B(s)} \begin{bmatrix} \hat{u}_k(s) \\ \hat{i}_k(s) \end{bmatrix}. \qquad (3.20)$$

The independent variable is not the (discrete) time but the *index of a section*, discrete spatial coordinate. Furthermore, unlike in the standard state space model for a lumped LTI system, the state matrix (labeled B in this case) is not just a constant real matrix, but it is parameterized by the complex variable s.

Note however, that since we do not keep the minus sign with i_{k+1} in (3.20), i_k is the current that leaves the right port of the k-th section and enters the connected left port of the $(k+1)$-the section, as illustrated in Fig. 3.6 and Fig. 3.7. This is a discrepancy that we have to keep in mind while interpreting the results arrived at in this section[2].

We can now view the task of relating the pair of variables $(\hat{u}_n, \hat{i}_n)$ to the pair $(\hat{u}_0, \hat{i}_0)$ as the task of solving the state-space model (3.20).

A standard procedure for analysis of linear state-space models is to convert the second-order system into a set of two independent first-order systems. This is accomplished by finding a transformation of state variables which will diagonalize the matrix $B(s)$.

First, we find the eigenvalues by solving for the roots of the characteristic polynomial

$$p(\lambda) = \det(\lambda I - B(s)) = \lambda^2 + (-2 - Z_1 Y_2)\lambda + 1, \qquad (3.21)$$

---

[2]We could have redefined the inverse chain matrix in (3.9) so that the positive direction for the current i_2 on the right (output) port of the two-port network is always out of the port (through the + terminal, but we wanted to stick to the conventions so that later some energy-related arguments can be made without additional changes. The price to pay is this temporary inconsistency in notation.

which gives these two eigenvalues

$$\lambda_1(s) = \frac{1}{2}\Big(2 + Z_1(s)Y_2(s)$$
$$- \sqrt{Z_1^2(s)Y_2^2(s) + 4Z_1(s)Y_2(s)}\Big),$$
$$\lambda_2(s) = \frac{1}{2}\Big(2 + Z_1(s)Y_2(s)$$
$$+ \sqrt{Z_1^2(s)Y_2^2(s) + 4Z_1(s)Y_2(s)}\Big). \tag{3.22}$$

where, thanks to the fact that the coefficient of the zero-th power of λ is one, we can immediately conclude that

$$\lambda_2(s) = \frac{1}{\lambda_1(s)}. \tag{3.23}$$

But the two eigenvalues are related also in another way

$$\lambda_2(s) = \lambda_1(-s). \tag{3.24}$$

In the lossless and normalized case ($L = C = 1$) the two eigenvalues are

$$\lambda_1(s) = \frac{1}{2}\left(2 + s^2 - s\sqrt{4 + s^2}\right), \tag{3.25}$$

$$\lambda_2(s) = \frac{1}{2}\left(2 + s^2 + s\sqrt{4 + s^2}\right). \tag{3.26}$$

The matrix $T(s)$ comprising two (column) eigenvectors is

$$T(s) = \begin{bmatrix} 1 & 1 \\ \frac{2Y_2}{Z_1Y_2 + \sqrt{Z_1^2Y_2^2 + 4Z_1Y_2}} & \frac{2Y_2}{Z_1Y_2 - \sqrt{Z_1^2Y_2^2 + 4Z_1Y_2}} \end{bmatrix}$$
$$= \begin{bmatrix} 1 & 1 \\ \frac{Y_2(s)}{\lambda_2(s) - 1} & \frac{Y_2(s)}{\lambda_1(s) - 1} \end{bmatrix} \tag{3.27}$$

In the lossless and normalized case it is

$$T(s) = \begin{bmatrix} 1 & 1 \\ \frac{2}{s + \sqrt{4 + s^2}} & \frac{2}{s - \sqrt{4 + s^2}} \end{bmatrix}. \tag{3.28}$$

Let's label the inverses of the entries in the second row as

$$Z_{r1} := \frac{Z_1Y_2 + \sqrt{Z_1^2Y_2^2 + 4Z_1Y_2}}{2Y_2}, \tag{3.29}$$

$$Z_{r2} := \frac{Z_1Y_2 - \sqrt{Z_1^2Y_2^2 + 4Z_1Y_2}}{2Y_2}. \tag{3.30}$$

The matrix vector relationship between the original and the new state variables is then

$$\begin{bmatrix} \hat{u}_k \\ \hat{i}_k \end{bmatrix} = \begin{bmatrix} 1 & 1 \\ Z_{r1}^{-1} & Z_{r2}^{-1} \end{bmatrix} \begin{bmatrix} \hat{u}_k^+ \\ \hat{u}_k^- \end{bmatrix}, \tag{3.31}$$

where $\hat{u}_k^+$ and $\hat{u}_k^-$ are new state variables.

The two functions Z_{r1} and Z_{r2} are related as

$$Z_{r1} Z_{r2} = -\frac{Z_1}{Y_2}, \tag{3.32}$$

which specializes in the lossless and normalized case (but more generally if $Y_2 = Z_1$) to

$$Z_{r1} = -\frac{1}{Z_{r2}}. \tag{3.33}$$

Moreover, in the lossless case[3] it also holds that

$$Z_{r2}(s) = -Z_{r1}(-s), \tag{3.34}$$

which can be rewritten compactly as in

$$Z_{r2} = -Z_{r1*}, \tag{3.35}$$

where the asterisk denotes *paraconjugate* of the given real function. More generally, recall (for example [7], page 70–71) that a paraconjugate function to some given function $Z(s)$ is defined as

$$Z_*(s) := \overline{Z(-\bar{s})}, \tag{3.36}$$

which reduces to

$$Z_*(s) = Z(-s) \tag{3.37}$$

for real functions. The reason for using a paraconjugate is that it agrees with the *complex conjugate* when the function is evaluated on the imaginary axis and yet it is an analytic function.

Note that the choice of the eigenvectors defining the $T(s)$ matrix was not unique—we can scale the columns arbitrarily. Nonetheless, for our particular choice the new state variables can be seen to have a dimension of voltage thanks to the normalized first row, and we have

$$\hat{u}_k(s) = \hat{u}_k^+(s) + \hat{u}_k^-(s). \tag{3.38}$$

Later we will see that these could be interpreted as "incident and reflected (voltage) waves" which will justify the notation.

---

[3]It may also hold in the lossy case, but I did not prove it

Using the functions Z_{r1} and Z_{r2}, the inverse matrix is

$$T^{-1} = \begin{bmatrix} \frac{Z_{r1}}{Z_{r1}+Z_{r2}} & \frac{Z_{r1}Z_{r2}}{Z_{r1}+Z_{r2}} \\ \frac{Z_{r2}}{Z_{r1}+Z_{r2}} & -\frac{Z_{r1}Z_{r2}}{Z_{r1}+Z_{r2}}, \end{bmatrix} \tag{3.39}$$

which, upon substitution yields

$$T^{-1} = \begin{bmatrix} \frac{1}{2}\left(1 + \frac{\sqrt{Z_1}\sqrt{Y_2}}{\sqrt{4+Z_1 Y_2}}\right) & \frac{\sqrt{Z_1}/\sqrt{Y_2}}{\sqrt{4+Z_1 Y_2}} \\ \frac{1}{2}\left(1 - \frac{\sqrt{Z_1}\sqrt{Y_2}}{\sqrt{4+Z_1 Y_2}}\right) & -\frac{\sqrt{Z_1}/\sqrt{Y_2}}{\sqrt{4+Z_1 Y_2}}. \end{bmatrix}. \tag{3.40}$$

The new (transformed) state variables then obey the discrete state-space model

$$\begin{bmatrix} \hat{u}_{k+1}^+(s) \\ \hat{u}_{k+1}^-(s) \end{bmatrix} = \underbrace{\begin{bmatrix} \lambda_1(s) & 0 \\ 0 & \lambda_2(s) \end{bmatrix}}_{\Lambda(s)} \begin{bmatrix} \hat{u}_k^+(s) \\ \hat{u}_k^-(s) \end{bmatrix}. \tag{3.41}$$

We now consider that there are in total n sections in the ladder. We want to relate the variables at the beginning (the left end) and the end (the right end) of the ladder using the diagonalized set of difference equations (3.41). Note that the variables to the left of the k-th section are indexed with the $(k-1)$ index

$$\hat{u}_k^+(s) = \lambda_1^k(s)\,\hat{u}_0^+(s), \tag{3.42}$$

$$\hat{u}_k^-(s) = \lambda_2^k(s)\,\hat{u}_0^-(s). \tag{3.43}$$

We may now use the freedom to pick an arbitrary section as the "initial" one (instead of $\hat{u}_0^-$) for the $\hat{u}_k^-$ variable and we choose the rightmost section (indexed n))

$$\hat{u}_k^-(s) = \lambda_2^{(k-n)}(s)\,\hat{u}_n^-(s), \tag{3.44}$$

$$= \lambda_1^{(n-k)}(s)\,\hat{u}_n^-(s). \tag{3.45}$$

where in the last equation we exploited the fact that $\lambda_2 = \lambda_1^{-1}$.

We now load the n-th (the right-most) section with some lumped impedance $Z_L(s)$ and we want to find the transfer function from $\hat{u}_0^+(s)$ to $\hat{u}_0^-(s)$. The first and the third transfer functions in the composed transfer function

$$\frac{\hat{u}_0^-(s)}{\hat{u}_0^+(s)} = \frac{\hat{u}_0^-(s)}{\hat{u}_n^-(s)}\frac{\hat{u}_n^-(s)}{\hat{u}_n^+(s)}\frac{\hat{u}_n^+(s)}{\hat{u}_0^+(s)} \tag{3.46}$$

are particularly easy to evaluate thanks to the decoupled (diagonalized) state matrix

$$\frac{\hat{u}_n^+(s)}{\hat{u}_0^+(s)} = \lambda_1^n(s) = \lambda_2^{-n}(s), \tag{3.47}$$

$$\frac{\hat{u}_0^-(s)}{\hat{u}_n^-(s)} = \lambda_1^n(s) = \lambda_2^{-n}(s). \tag{3.48}$$

The middle one is only a bit more tedious. We need to infer the relationship between $\hat{u}_n^+$ and $\hat{u}_n^-$ from that of $\hat{u}_n$ and $\hat{i}_n$. The latter coupling is given by (recall the our agreement here on the current going out of the last port and into the load, that is, $i_n = i_{\mathrm{L}}$)

$$\hat{u}_n(s) = Z_{\mathrm{L}}(s)\,\hat{i}_n(s), \tag{3.49}$$

which yields

$$\hat{u}_n^+ = \frac{1}{Z_{\mathrm{r}1} + Z_{\mathrm{r}2}}\left(Z_{\mathrm{r}1}Z_{\mathrm{L}} + Z_{\mathrm{r}1}Z_{\mathrm{r}2}\right)\hat{i}_n, \tag{3.50}$$

$$\hat{u}_n^- = \frac{1}{Z_{\mathrm{r}1} + Z_{\mathrm{r}2}}\left(Z_{\mathrm{r}2}Z_{\mathrm{L}} - Z_{\mathrm{r}1}Z_{\mathrm{r}2}\right)\hat{i}_n. \tag{3.51}$$

The needed third transfer function $\hat{u}_n^-(s)/\hat{u}_n^+(s)$ is then

$$\Gamma_{\mathrm{L}} = \frac{Z_{\mathrm{r}2}}{Z_{\mathrm{r}1}}\frac{Z_{\mathrm{L}} - Z_{\mathrm{r}1}}{Z_{\mathrm{L}} - Z_{\mathrm{r}2}}. \tag{3.52}$$

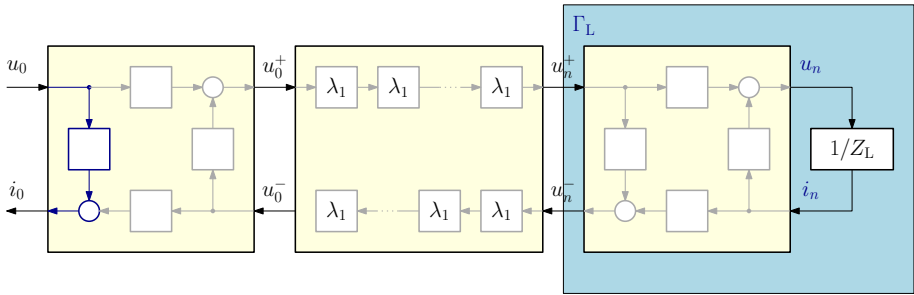This diagonal decomposition can also be visualized in the block diagram in Fig. 3.9

Figure 3.9: Diagonalized inverse hybrid description of a loaded ladder. The highlighted (blue) direct path from u_0 to i_0 is what is left after the path from u_n^+ to u_n^- (in the light blue block) is left open by a "suitable" impedance

In order to find the transfer functions for the two nondiagonal blocks in Fig. 3.9, we notice first that the full ladder model in the factorized chain format is

$$\begin{bmatrix} \hat{u}_n(s) \\ \hat{i}_n(s) \end{bmatrix} = B^n(s) \begin{bmatrix} \hat{u}_0(s) \\ \hat{i}_0(s) \end{bmatrix} \tag{3.53}$$

$$= T(s)\, \Lambda^n(s)\, T^{-1}(s) \begin{bmatrix} \hat{u}_0(s) \\ \hat{i}_0(s) \end{bmatrix}. \tag{3.54}$$

The transfer function matrix for the left block is then

$$\begin{bmatrix} \hat{i}_0 \\ \hat{u}_0^+ \end{bmatrix} = \begin{bmatrix} Z_{r1}^{-1} & Z_{r2}^{-1} - Z_{r1}^{-1} \\ 1 & -1 \end{bmatrix} \begin{bmatrix} \hat{u}_0 \\ \hat{u}_0^- \end{bmatrix}, \tag{3.55}$$

which can be modified after invoking (3.32) into

$$\begin{bmatrix} \hat{i}_0 \\ \hat{u}_0^- \end{bmatrix} = \begin{bmatrix} -\frac{Y_2}{Z_2} Z_{r2} & -\frac{Y_2}{Z_2}(Z_{r1} - Z_{r2}) \\ 1 & -1 \end{bmatrix} \begin{bmatrix} \hat{u}_0 \\ \hat{u}_0^- \end{bmatrix} \tag{3.56}$$

$$= \begin{bmatrix} \frac{-Z_1 Y_2 + \sqrt{Z_1^2 Y_2^2 + 4 Z_1 Y_2}}{2 Z_1} & -\frac{\sqrt{Z_1^2 Y_2^2 + 4 Z_1 Y_2}}{Z_1} \\ 1 & -1 \end{bmatrix} \begin{bmatrix} \hat{u}_0 \\ \hat{u}_0^- \end{bmatrix}, \tag{3.57}$$

where the last equality is due to (3.29).

Similarly, we can find the individual transfer functions for the right block in Fig. 3.9.

The signal flow diagram in Fig. 3.9 shows that the signal path to the right of the diagonal block, that is, the transfer from u_n^+ to u_n^- can be broken by a suitable choice of the load impedance Z_L. Why should we do that? Identical reasoning can be used as for the spatially continuous version of our setup—transmission line—in which case the interruption of the signal path corresponds to prevention of reflections at line termination. The particular impedance is called *matching impedance*. That is where the notation and terminology for the new variables (u^+ and u^-, incident and reflected (voltage) waves, respectively) comes from. For a ladder, the condition for "no reflection" at the right end (on the load side) is obtained by setting (3.52) to zero.

Since both the numerator and denominator are just affine functions of Z_L, we can only search for the value of Z_L that set the numerator to zero. The solution

is given by

$$Z_{\mathrm{L}} = Z_{\mathrm{r}1} \tag{3.58}$$

$$= \frac{\sqrt{4Z_1Y_2 + Z_1^2Y_2^2} + Z_1Y_2}{2Y_2} \tag{3.59}$$

$$= -\frac{Z_1}{Y_2}\frac{1}{Z_{\mathrm{r}2}} \tag{3.60}$$

$$= \frac{2Z_1}{\sqrt{4Z_1Y_2 + Z_1^2Y_2^2} - Z_1Y_2}. \tag{3.61}$$

Since we have (arbitrarily) enforced u_n to be the input to the load and i_n the output from the load, we will actually need the inverse of the load impedance $Z_{\mathrm{L}}(s)$, that is, the admittance $Y_{\mathrm{L}}(s)$

$$Y_{\mathrm{L}} = \frac{\sqrt{4Z_1Y_2 + Z_1^2Y_2^2} - Z_1Y_2}{2Z_1}. \tag{3.62}$$

For the lossless case, $Z_1(s) = Ls$ and $Y_2(s) = Cs$

$$Y_{\mathrm{L}} = \frac{\sqrt{4LCs^2 + L^2C^2s^4} - LCs^2}{2Ls} \tag{3.63}$$

$$= \frac{\sqrt{4LC + L^2C^2s^2} - LCs}{2L}. \tag{3.64}$$

Finally, for the lossless and normalized case ($L = C = 1$) we get

$$Y_{\mathrm{L}}(s) = 1/2\left(\sqrt{4 + s^2} - s\right), \tag{3.65}$$

which evaluates on the imaginary axis ($s = \jmath\omega$, $\jmath = \sqrt{-1}$) to

$$Y_{\mathrm{L}}(\jmath\omega) = 1/2\left(\sqrt{4 - \omega^2} - \jmath\omega\right). \tag{3.66}$$

where principal branch of the square root function is considered. The Nyquist and Bode plots are in Fig. 3.10a and Fig. 3.11a.

The load is passive and causal (with the voltage set as the input to the load).

Note the very peculiar property of this dynamical system: its gain remains exactly equal to one up to a certain frequency (2 rad/s in our normalized case) and then rolls off at the rate that ultimately comes close to that of a first-order system, that is -20db per decade. Similarly, the phase lag is constant above the given frequency. Hence, it can be (reasonably) approximated using a rational first-order filter, which is shown in the Bode plots too.

(a) Irrational $Y_{\mathrm{L}}(\jmath\omega)$, $\omega \in (0, \infty)$, the principal branch of the square root

(b) Irrational $Y_{\mathrm{L}}(\jmath\omega)$, $\omega \in (0, \infty)$, the negative branch of the square root
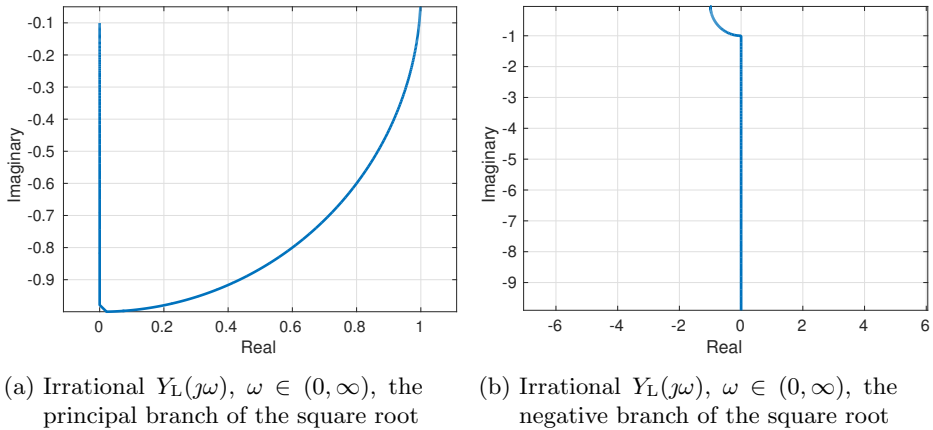
Figure 3.10: Nyquist plots

Note that the square root function for a complex argument (as used in (3.66)) also has another (negative) branch, which yields another function that perfectly satisfies the requirement of a frequency response

$$Y_{\mathrm{L}}(\jmath\omega) = 1/2 \left(-\sqrt{4 - \omega^2} - \jmath\omega \right). \tag{3.67}$$

The corresponding Nyquist and Bode plots are in Fig. 3.10b and Fig. 3.11b, respectively. The response reveals the corresponding transfer function is not causal and not passive.

Simulation example for an LC ladder

We have already mentioned that our analysis mimics the standard analysis performed for the spatially continuous counterpart of our setup—a transmission line. The particular load impedance that can be found following the diagonalization procedure guarantees that there will be no reflections of waves on the load side. It need not be immediately obvious if such interpretation can be given to the lumped version of the results. After all, one might argue that the concept of a wave (hence its reflection) has no justification in the lumped setting. We obtain some insight into this by means of a numerical simulation.

Five L-sections, each composed just of a series inductor and shunt capacitor, were connected into a ladder. A step in the voltage was applied on the input port (the left side of the ladder) and voltages on all the sections were simulated. In Fig. 3.12, no matching impedance on the load side (the right end) was attached. A propagation of the input signal to the right is recognizable during the first few

(a) Irrational $Y_{\mathrm{L}}(\jmath\omega)$ (blue) and a rational first-order filter (red)

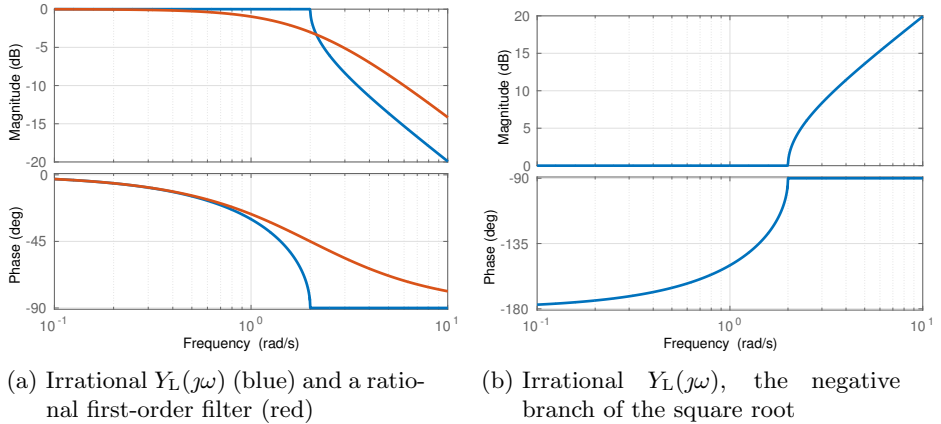(b) Irrational $Y_{\mathrm{L}}(\jmath\omega)$, the negative branch of the square root

Figure 3.11: Magnitude frequency plots

seconds of simulation. The resulting oscillatory behavior can then be interpreted as a superposition of the incident and reflected (voltage) waves. In Fig. 3.13a, a first-order approximation to the irrational matching impedance was attached to the right end of the ladder. Significant attenuation of oscillations is visible, which could be attributed to almost no reflections. Finally, in Fig. 3.13b we only used a real impedance, a resistor, which only approximates the matching impedance at steady state (at zero frequency). Almost no impact on the performance is visible (although for some other inputs this could be more visible).

3.5 Iterative impedances and LFT for chains

The simulation results suggest that the for the particular choice of the load impedance, the oscillations are eliminated (or at least significantly reduced). Hence it seems worth examining this kind of loading a bit more. It also turned out that when the ladder is loaded with such impedance, its input impedance is identical to the load impedance. To see this, note that the direct signal path from u_0 to i_0 highlighted in Fig. 3.9 and represented by the (1,1) entry in the matrix transfer function (3.57), which is what is left after the signal path from u_n^+ to u_n^- is broken, agrees with Y_{L} given in (3.62). This is a remarkable observation. It means that the dynamics of the ladder is transparent (invisible) from the input port and only the dynamics of the load can be sensed. This observation lead to the introduction of the concept of *iterative impedances* in literature on electrical multiport networks (see, for example, [42], page 177).

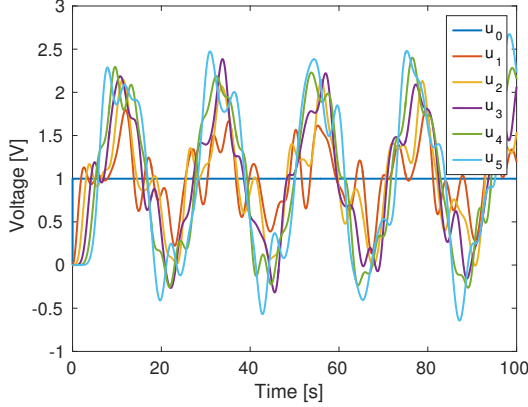It is now time to switch the language back to the one used in the control

Figure 3.12: Simulation responses of voltages at individual sections of an LC ladder with 5 sections. Stepwise voltage applied to the first section. Open circuit on the load side—huge oscillations

theory. We have already stated in Sec. 3.2 that we can view the problem of finding the load impedance as the task of designing a feedback controller with a transfer function K that closes the "generalized feedback loop" as characterized by the lower linear fractional transformation. For that we generally need the overall transfer function matrix. However, if we plan to plug in the "matching controller" into the feedback loop, the situation is much simpler.

The simplification stems from the definition of an iterative impedance for the whole ladder: the same iterative impedance must work for a single section too! That is, we do not even have to find the model for the full ladder to design a "matching controller". We can just use a single section as the model on which we base the design. The LFT setup is in Fig. 3.14.

The condition for an iterated impedance (or admittance in our case because we have chosen u_0 as the input) can be formally stated as

$$K = \mathcal{F}_{\text{lower}}(G, -K), \tag{3.68}$$

where G for a single section is given by (3.5). Note the minus sign with the controller K, which reflects the fact that while adhering to the definition of inverse hybrid matrix (3.5), the current i_n is into the $+$ terminal of the last port; the current through the load then needs to be taken with the negative sign. Alternatively, the inverse hybrid matrix G can be redefined so that i_n goes away from the port and into the load.

The equation (3.68) expands to the quadratic equation

$$Z_1 K^2 + Z_1 Y_2 K - Y_2 = 0. \tag{3.69}$$
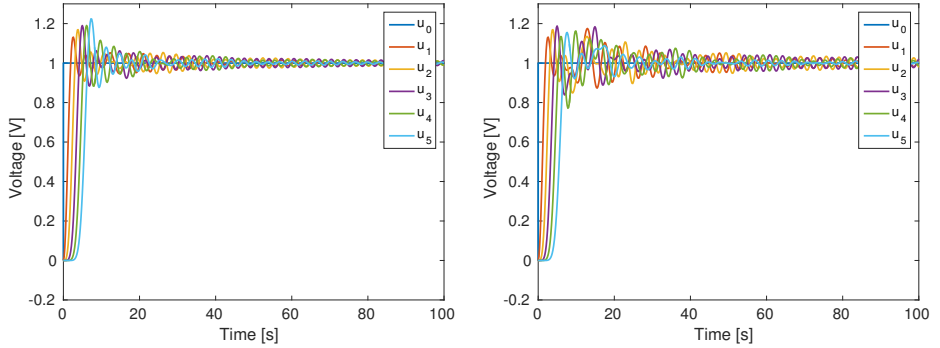
(a) Rational approximation to the "matching impedance" attached to the end section

(b) Real resistor approximating the matching impedance at steady state attached

Figure 3.13: Simulation responses of voltages at individual sections of an LC ladder with 5 sections. Stepwise voltage applied to the first section.
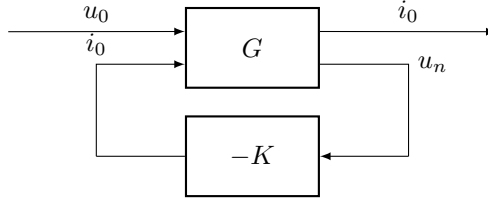

Figure 3.14: Lower linear fractional transformation of a single section (described by an inverse hybrid matrix transfer function G) with respect to the controller (admittance K)

This quadratic (in K) equation has two solutions

$$K_1 = \frac{-Z_1 Y_2 + \sqrt{Z_1^2 Y_2^2 + 4 Z_1 Y_2}}{2 Z_1} \tag{3.70}$$

$$K_2 = \frac{-Z_1 Y_2 - \sqrt{Z_1^2 Y_2^2 + 4 Z_1 Y_2}}{2 Z_1}. \tag{3.71}$$

We can immediately recognize K_1 as our matching admittance Y_L derived in the previous section while relying on the principal square root. The K_2 solution then corresponds to the negative branch of the square root.

Let's summarize the several interesting (and perhaps even striking) properties of the new controller:

1. Even for the lossless system the matching impedance is dynamical. Recall that for a lossless transmission line, which can be viewed as a continuum version of our lumped chain (more on this later), the matching impedance is real—just a resistor is enough. In order words, for a lossless chain even a proportional controller is not enough to achieve a perfect cancellation of the oscillations. The simulations suggest, though, that reasonable reduction in oscillations can be attained just with a proportional controller.

2. The matching impedance is irrational. This will certainly have an impact on implementation. Some approximation schemes will have to be invoked.

3. The matching impedance does not depend on the number of sections! This is a striking property. Even if we add more sections into the ladder, the matching impedance (hence admittance too, the controller) does not have to be redesigned. Single quadratic equation has to be solved using the model of a single section. As we will see later, some other control schemes such as $\mathcal{H}_\infty$-optimal control suffer from the fact that the order of the chain and hence the order of the resulting controller grows as additional subsystems are inserted into the chain.

4. the matching impedance guarantees closed-loop stability since it is passive (and the system is passive too).

3.6 Asymptotic behavior of chains (ladders)

Our primary motivation for the whole work is to understand better how the control design scales with the growing number of subsystems in the chain (or sections in the ladder). We consider two separate scenarios. First, sections are simply added to the ladder. Second, sections are added after the parameters were scaled by the number of sections in the ladder. The latter approach yields a discrete approximation of the spatially continuous version of our problem—a transmission line.

3.6.1 Number of sections is growing, no scaling of sections

The input impedance for an unterminated single section ($Z_\mathrm{L}(s) = 0$) is

$$Z_\mathrm{input}^{(1)}(s) = Z_1(s) + \frac{1}{Y_2(s)}, \tag{3.72}$$

while for two (cascaded) section it extends to

$$Z_\mathrm{input}^{(2)}(s) = Z_1(s) + \frac{1}{Y_2(s) + \frac{1}{Z_1(s) + \frac{1}{Y_2(s)}}}. \tag{3.73}$$

The pattern is now obvious—the input impedance for an unloaded (unterminated) ladder with k sections is given by the (finite) *continued fractions*

$$Z_{\text{input}}^{(k)}(s) = Z_1(s) + \cfrac{1}{Y_2(s) + \cfrac{1}{Z_1(s) + \cfrac{1}{Y_2(s) + \cfrac{1}{Z_1(s) + \dots}}}}. \tag{3.74}$$

Note that this gives us the $(1,1)$ term of the $G(s)$ inverse hybrid matrix. Similarly we could encode the evolution of other elements of this matrix as the number of sections grows.

The Fig. 3.15a and 3.15b show the location of the open-loop poles and zeros for a ladder composed of 2 and 5 sections, respectively. Then the Fig. 3.16a and 3.16b show magnitude frequency responses.
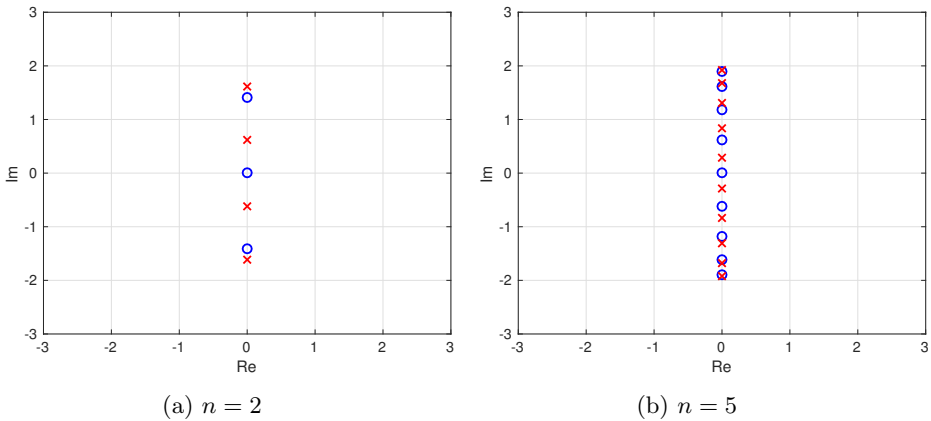

(a) $n = 2$ (b) $n = 5$

Figure 3.15: Poles and zeros for the input impedance for a lossless and normalized n-section ladder. The red crosses are poles, the blue dots are zeros

Similar comparison can be done for frequency responses—see the Fig. 3.16a and 3.16b. We observe that as the number of sections grows, no resonant peak appears at frequencies above 2 rad/s. Instead, the lowest resonant frequency decreases and the density of resonant peaks in the frequency interval $\omega \in [0,2]$ grows.

3.6.2 Sections are scaled while the ladder's length is growing

Now we will investigate a different kind of asymptotic scenario. We will again consider the lossless case ($R = G = 0$) and focus on the $(1,1)$ element, which determines the open-loop dynamics. After considering a ladder containing just a

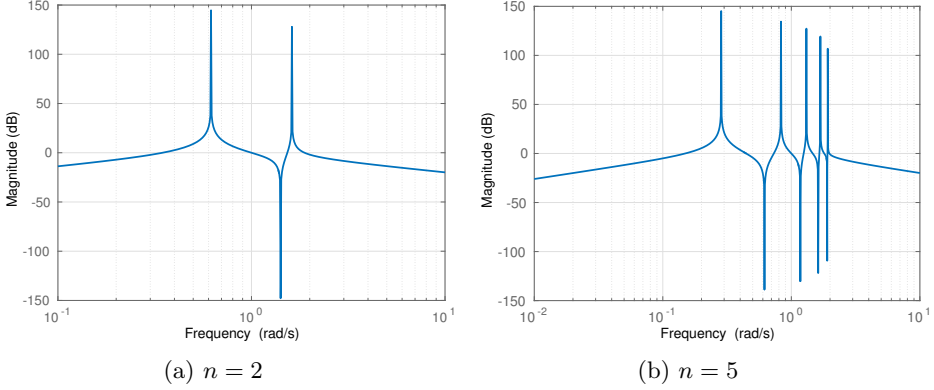(a) $n = 2$ (b) $n = 5$

Figure 3.16: Magnitude frequency response for the input impedance for a lossless and normalized n-section ladder

single section characterized by a series inductance L and shunt capacitance C, we add another section, but this time we adjust the parameters L and C so that the new ladder can be regarded as a higher accuracy model of a transmission line. That is, the continued fractions for the input impedance with $k = 2$ sections is then

$$Z_{\text{input}}^{(2)}(s) = \frac{L}{2}s + \cfrac{1}{\frac{C}{2}s + \cfrac{1}{\frac{L}{2}s + \frac{1}{\frac{C}{2}s}}}. \tag{3.75}$$

The evolution of the pole-zero pattern as a function of the number of sections is now dramatically different. We only show it here for $n = 10$ but compare it with the frequency response of the lossless and normalized linear transmission line.

The lossless and normalized $(R = G = 0, L = C = 1)$ transmission line's open-loop transfer function is

$$g_{11}(s) = \frac{\sinh s}{\cosh s}. \tag{3.76}$$

There are apparently an infinite number of open-loop poles and zeros of g_{11} for the transmission line and these are given by
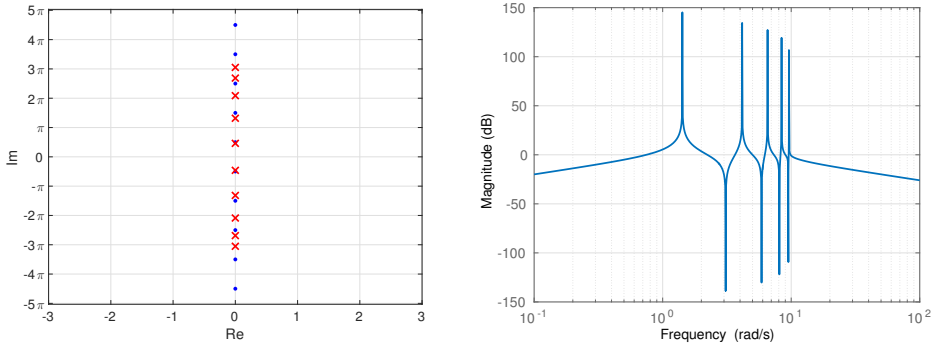
$$P = \left\{ s \in \mathbb{C} : s = \jmath\pi m + \jmath\frac{\pi}{2},\ m \in \mathbb{Z} \right\} \tag{3.77}$$

and

$$Z = \left\{ s \in \mathbb{C} : s = \jmath\pi m,\ m \in \mathbb{Z} \right\}, \tag{3.78}$$

In order to avoid cluttering, we only show the open-loop poles and skip the open-loop zeros in Fig. 3.17a. On the other hand, (some) open-loop poles of the transmission line transfer function are indicated too (they extend towards the infinity).

(a) Open-loop poles of the input impedance. The red crosses are the poles. The blue dots distributed equidistantly are the open-loop poles of the irrational transfer function corresponding to a unit-length lossless transmission line

(b) Magnitude frequency response

Figure 3.17: Open-loop poles and magnitude frequency response for the input impedance for a lossless and scaled ladder with 5 sections

Obviously, by appropriately scaling the physical parameters of the individual section as the number of sections in the ladder grows, the ladder becomes more and more accurate finite-dimensional approximation of an infinite-dimensional transmission line. The lower resonant frequency remains intact but other resonant peaks appear at higher frequencies. The frequency content spreads towards higher and higher frequencies and yet the poles (and zeros) remain isolated points in the complex plane.

3.7 $\mathcal{H}_\infty$-optimal control for chains

Besides the controller that realizes the impedance matching, we have already mentioned in Sec. 3.2 another and very standard optimal control problem in Sec. 3.2—the popular $\mathcal{H}_\infty$-optimal control design.

Here we will build the G transfer matrices of increasing order by adding sec-

tions, one by one, and design an $\mathcal{H}_\infty$-optimal controller. The first few G's are

$$G_1(s) = \begin{bmatrix} \frac{s}{1+s^2} & \frac{1}{1+s^2} \\ \frac{1}{1+s^2} & -\frac{s}{1+s^2} \end{bmatrix} \qquad (3.79)$$

$$G_2(s) = \begin{bmatrix} \frac{s(2+s^2)}{1+3s^2+s^4} & \frac{1}{1+3s^2+s^4} \\ \frac{1}{1+3s^2+s^4} & -\frac{s(2+s^2)}{1+3s^2+s^4} \end{bmatrix} \qquad (3.80)$$

$$G_3(s) = \begin{bmatrix} \frac{s(3+4s^2+s^4)}{1+6s^2+5s^4+s^6} & \frac{1}{1+6s^2+5s^4+s^6} \\ \frac{1}{1+6s^2+5s^4+s^6} & -\frac{s(3+4s^2+s^4)}{1+6s^2+5s^4+s^6} \end{bmatrix} \qquad (3.81)$$

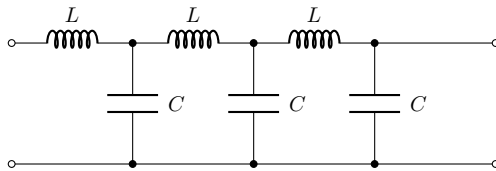The G_3 matrix thus corresponds to the lossless ladder in Fig. 3.18.

Figure 3.18: A lossless ladder composed of a three L-sections consisting of an inductor (inductance L) and capacitor (capacitance C)

The above is in the format compatible with the positive feedback assumption of many numerical solvers. Currently we can only solve this series of $\mathcal{H}_\infty$ optimizations by invoking a numerical solver. Namely, we used the `hinf()` function that can be found in Robust Control Toolbox for Matlab. We used it with the option `'lmi'`, which tells the function to used the algorithm based on linear matrix inequalities. Magnitude frequency plots for the sequence of the achieved closed-loop transfer functions is in Fig. 3.19. It is a striking observation that after adding just a few sections (5 in total or so), the closed-loop transfer function starts resembling the irrational transfer function that we studied earlier (see Fig. 3.11a). The irrational transfer function corresponding to the closed-loop response of a ladder loaded with an iterative impedance is hardly visible because it almost perfectly coincides with the achieved F_5—the convergence is very fast.

In Fig. 3.20a we can see the evolution of the achieved norms of the closed-loop transfer functions.

The convergence is indeed very fast, as the logarithmic plot of the evolution of the error in Fig. 3.20a shows. Asymptotically it looks linear in the logarithmic scale, hence we can suspect (hope for) an exponential decay. It is very fast!

We can run the whole sequence of control design problems for the case when the parameters of the individual section are scale if the ladder is augmented with other sections. The sequence of a few closed-loop magnitude frequency responses
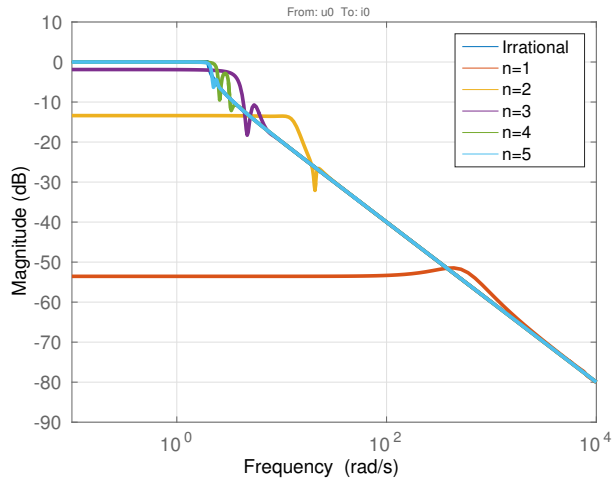
Figure 3.19: Magnitude frequency response for closed-loop transfer functions F_n for ladders of growing n (the number of sections) and with their corresponding $\mathcal{H}_\infty$-optimal controller

is in Fig. 3.21. Unlike in the previous—unscaled—case, here we observe that as the number of sections is increased (whiled the section's parameters are scaled), the bandwidth of the achieved closed-loop transfer function grows (although it will never converge to the model of a transmission line, which has an infinite bandwidth—it is a real constant).
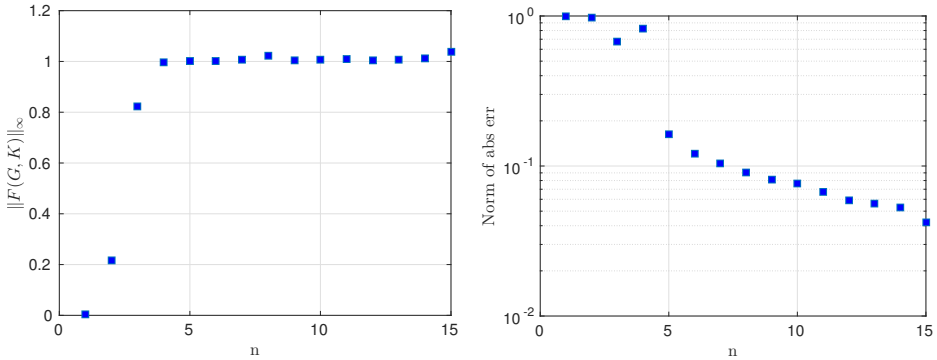
The convergence of this closed-loop transfer function to the irrational transfer function derived for the particular number of sections (recall that the parameters are scaled by n) looks similarly fast as in the unscaled case, see Fig. 3.22

It is purely based on these empirical (numerical) observations that we make a conjecture about the relationship between the $\mathcal{H}_\infty$-optimal control design for a ladder and the (irrational) iterative impedance (admittance).

Theorem 2. *For a lossless ladder composed of finite number of sections, the closed-loop transfer function obtained with an $\mathcal{H}_\infty$-optimal feedback controller converges to the irrational iterative transfer function as the number of sections in the ladder grows. Furthermore, the convergence is exponential.*

Proof. Currently missing. □

(a) Evolution of the achievable $\mathcal{H}_\infty$ norm of the closed-loop system as the number n of sections in the ladder grows

(b) The $\mathcal{H}_\infty$ norm of the error between the optimal closed-loop transfer function and the irrational transfer function as n grows

Figure 3.20: Evolution of the norms as the number n of sections grows

3.8 Analogy with the mechanical chain of masses, springs and dampers

The results derived in the previous sections are tailored to electrical ladders (and electrical transmission lines). How do these translate into other physical domains such as the mechanical one? We are going to show that the results on electrical ladders have immediate interpretation for chains of masses interconnected with springs (and dampers in the lossy case). We invoke the powerful Maxwell analogy among physical domains, which views the electrical voltage as the same kind of physical variable as the force, and similarly the electrical current of the same kind as the velocity. Note that there is alternative analogy, sometimes referred to as *across-through* analogy, in which current is of the same kind as force, and which is particularly popular in mechatronics because it does not extend easily to other physical domains such as hydraulics. Our preference for the former is supported by [9] as it might later enable making reference to some fundamental thermodynamics arguments.

The Maxwell analogy is also exploited by the modeling methodology based on *power bond graphs*. Introduced by Paynter in 1950s [66], bond graphs evolved into a powerful tool with many excellent introductory texts such as [10] and [32]. The tutorial paper [22] can also serve well.
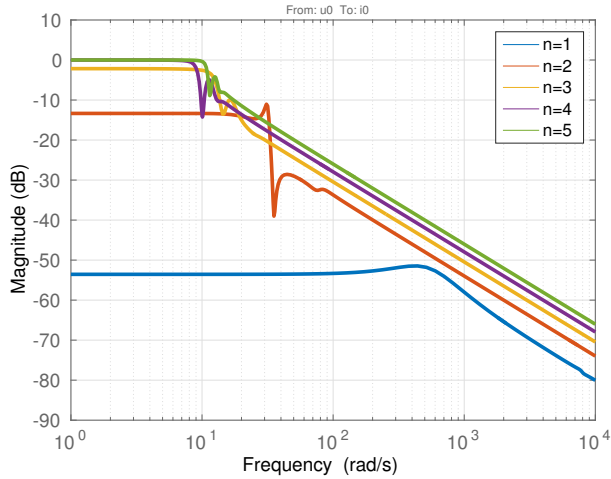
Figure 3.21: Magnitude frequency response for closed-loop transfer functions F_n for ladders of a growing number of sections and with their corresponding $\mathcal{H}_\infty$-optimal controller. The parameters of the sections are always scaled as another section is added

3.8.1 Lossy ladders and chains

The bond graph for the electrical ladder composed of three L-sections is in Fig. 3.23. We highlight the type-0 junctions since these correspond to the node voltages.

The bond graph for a mechanical chain composed of three identical masses interconnected with springs and dampers as in Fig. 1.2 is in Fig. 3.24. The input is the force acting on the first mass. Note that in order to make the mechanical scenario analogous to the electrical one, the last mass in the chain needs have a spring and damper interconnection with the reference frame; it cannot be just floating. We highlight the type-1 junctions since these correspond to distinct velocities.

Obviously, the two bond graphs do not match. In the mechanical bond graph the "resistor" corresponding to the relative friction (the dashpots between the neighbor masses) enters the graph in a different way than the shunt resistor $(1/G)$ in the electrical bond graph. An L-section analogous to the mechanical mass-spring-damper chain is in Fig. 3.25
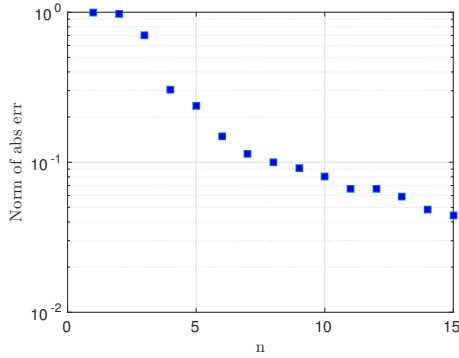
Figure 3.22: Evolution of the $\mathcal{H}_\infty$ norm of the error between the optimal closed-loop transfer function and and the irrational transfer function as the number of sections in the ladder grows (while the parameters of the sections are scaled)
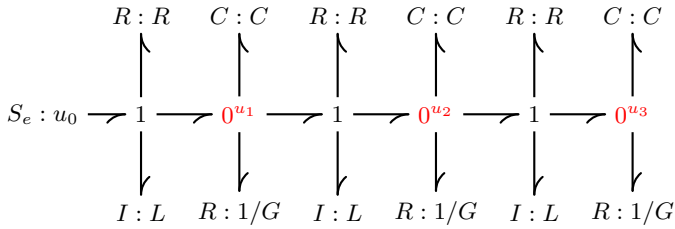

Figure 3.23: Bond graph for an electrical ladder composed of three L-sections. The input is the voltage u_0.

The series impedance and shunt admittance are thus redefined to

$$Z_1(s) = ms + b_\mathrm{a}, \tag{3.82}$$

$$Y_2(s) = \frac{1}{b_\mathrm{r} + \frac{k}{s}} = \frac{s}{b_\mathrm{r}s + k}. \tag{3.83}$$

We include yet another word of warning here, perhaps redundant, that relates to our choice of physical analogy (Maxwell). Some engineers well entrenched in the domain of electromechanical systems might be more familiar with the alternative *across-through* analogy, which has an impact on the definition of the impedances and admittances here.
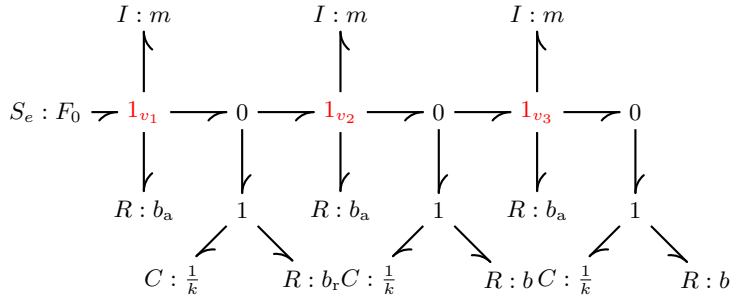
Figure 3.24: Bond graph for an mechanical chain composed of three masses interconnected with springs and dampers. The input is the force F_0 on the first mass.
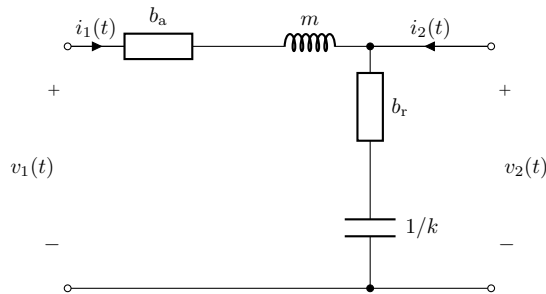

Figure 3.25: A single L-section corresponding to the mass-spring-damper system

3.8.2 Lossless ladders and chains

For the lossless mass-spring chain, however, the match with a lossless ladder reappears. The bond graph for the lossless case, common for the electrical and mechanical domains, is in Fig. 3.26. We intentionally do not perform all the possible reduction of the graph (in particular, canceling the type-0 junction for u_3) with the motivation to keep it clear where a possible load impedance should come.

The impedance $Z_1(s)$ and the admittance $Y_1(s)$ corresponding to a single lossless L-section (analogous to a lossless mass-spring chain) are

$$Z_1(s) = ms, \tag{3.84}$$
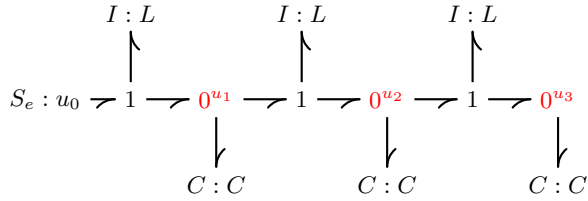
$$Y_2(s) = \frac{s}{k}. \tag{3.85}$$

Figure 3.26: Bond graph for a lossless electrical ladder composed of three L-sections. The input is the voltage u_0. The bond graph also describes a chains of three masses interconnected with springs (no dampers) with a force exerted on the first mass and a spring placed between the last mass and a reference frame

3.8.3 Loading the lossless mass-spring chain

Now, let's see where the matching impedance $Z_L(s)$ fits within the bond graph. In the lossless case as we have just analyzed, it fits as described in Fig. 3.27.
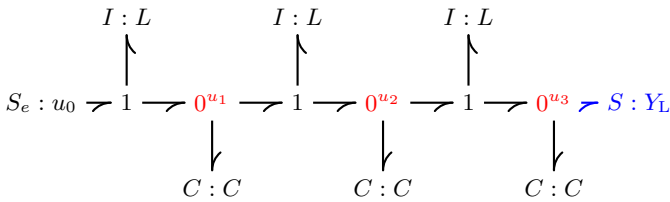

Figure 3.27: Bond graph for a lossless electrical ladder composed of three L-sections. The input is the voltage u_0. The blue bond at the end attaches a load (sink) characterized by its impedance $Z_L(s)$. The bond graph also describes a chains of three masses interconnected with springs (no dampers) with a force exerted on the first mass and a spring placed between the last mass and a reference frame.

Fitting the results on impedance matching derived for the lossless electrical ladder to the lossless mechanical chain is straightforward. Analogous to the inductance L we have a mass m and analogous to the capacitance C we have a string compliance, which is defined as the inverse of the spring constant k. Hence the mechanical version of the matching impedance is

$$Z_L(s) = \frac{2ms}{-\frac{m}{k}s^2 + \sqrt{\frac{m}{k}}s\sqrt{4 + \frac{m}{k}s^2}}. \tag{3.86}$$

After introducing

$$\omega_{\mathrm{n}} = \sqrt{\frac{k}{m}} \tag{3.87}$$

we can write the matching load admittance as

$$Y_{\mathrm{L}} = \frac{\sqrt{1 + \left(\frac{s}{2\omega_{\mathrm{n}}}\right)^2} \frac{s}{\omega_{\mathrm{n}}} - \frac{1}{2}\left(\frac{s}{\omega_{\mathrm{n}}}\right)^2}{ms}. \tag{3.88}$$

This format of the result will be useful later when we discuss the similarity of the proposed approach to the existing approaches, namely the O'Connor's *wave transfer function* approach.

3.8.4 Unanchored mass-spring chain

There is another setup for a mechanical mass-spring-damper chain which is in some sense dual to the one just discussed. We illustrate it in Fig. 3.28
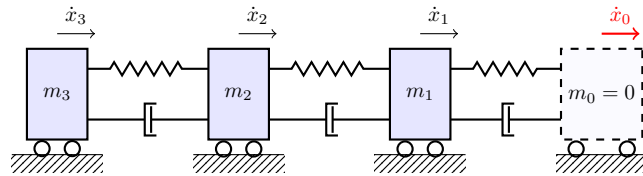

Figure 3.28: Multiple masses interconnected with springs and dampers. The first mass can be virtual, it travels at a prescribed velocity. The last mass is floating

The power bond graph corresponding to this chain assuming absence of losses is in Fig. 3.29.

If the bond graph is not enough, then the electrical circuit schematics in Fig. 3.30 will give the full analogy

3.9 Asymmetric chains

So far the discussion revolved around system for which the coupling with the neighbors was perfectly symmetric. And yet one of our initial motivations for exploring the whole approach stems from vehicular platooning, in which asymmetric interactions between the vehicles are common. At first it might seem that the energy-based framework used in this work cannot offer much for asymmetric chains. After all, one can hardly think of a chain of particles interconnected with
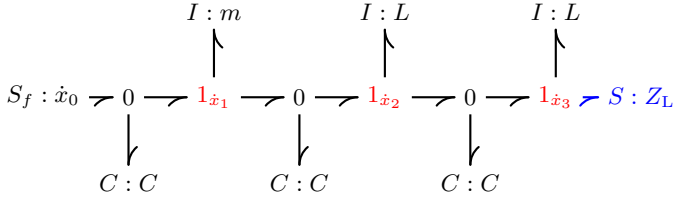
Figure 3.29: Bond graph for a lossless mass-spring chain with the velocity of the 0-th vehicle as the control input and the last mass floating. Analogously, it can be viewed as a model of a lossless ladder with the current entering the first section as the input
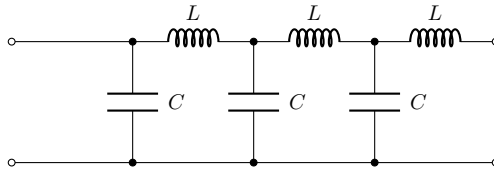

Figure 3.30: A lossless ladder composed of a few reversed L-sections consisting of an inductor (inductance L) and capacitor (capacitance C)

some special strings which would deny the third Newtons law (the action is equal in magnitude to the reaction). However, the electrical engineering offers a very systematic approach to the asymmetric chains (ladders) as well—*active networks*.

Consider the simplest possible vehicular platooning setup of Fig. 1.6, in which each vehicle measures its distance from the immediate predecessor and adjusts its throttle (hence force on the vehicle) so that some prescribed intervehicular distance is kept. Obviously, the coupling is only one-directional—whatever disturbances are only propagated away from the leader towards the tail of the platoon. According to this model, the vehicle's control strategy does not care about the vehicle(s) behind.

Now consider an active ladder composed of simple active sections as in Fig. 3.31. Although it does not immediately correspond to the predecessor following model, it does exhibit the one-directional propagation of signal, as needed in models of vehicular platoon.

The inverse chain matrix of the voltage follower (also voltage buffer) is

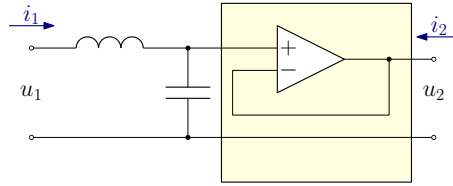$$B_2(s) = \begin{bmatrix} 1 & 0 \\ 0 & 0 \end{bmatrix}, \tag{3.89}$$

Figure 3.31: Voltage follower appended to an LC section in order to create an asymmetric section

which gives the combined inverse chain matrix model of the asymetric section

$$\begin{bmatrix} \hat{u}_2(s) \\ -\hat{i}_2(s) \end{bmatrix} = B_2(s)\, B_1(s) \begin{bmatrix} \hat{u}_1(s) \\ \hat{i}_1(s) \end{bmatrix} \tag{3.90}$$

$$= \begin{bmatrix} 1 & -Ls \\ 0 & 0 \end{bmatrix} \begin{bmatrix} \hat{u}_1(s) \\ \hat{i}_1(s) \end{bmatrix}. \tag{3.91}$$

The fact that the only way to introduce asymmetry into the system was to have a generator there, seems fundamental. It is also related to the property of *reciprocity*. But we will not elaborate on it in this work. It is certainly one of next directions to explore, though.

3.10 Relationship with existing results

3.10.1 Chain-scattering approach to $\mathcal{H}_\infty$-optimal control design

The task of minimizing the $\mathcal{H}_\infty$ norm of the closed-loop transfer function in Fig. 2.1, which is given by (2.2) recapitulated below

$$\mathcal{F}_{\text{lower}}(G, K) = G_{11} + G_{12}K(I - G_{22}K)^{-1}G_{21} \tag{3.92}$$

is far from easy and most papers on robust control in 1980s and 1990s revolved around this computational issue. In the late 1980s, one (another) particular framework for $\mathcal{H}_\infty$-optimal control appeared in the control theory literature. Rather then characterizing the response of the generalized plants to the inputs w and u, find the mathematical model which would flip the causality of the first input (w) and the second output (y). What we are heading for is a transfer function matrix C that relates the new "inputs" and "outputs" as

$$\begin{bmatrix} \hat{z}(s) \\ \hat{w}(s) \end{bmatrix} = \begin{bmatrix} C_{11}(s) & C_{12}(s) \\ C_{21}(s) & C_{22}(s) \end{bmatrix} \begin{bmatrix} \hat{u}(s) \\ \hat{y}(s) \end{bmatrix}. \tag{3.93}$$

The entries of the matrix C relate to those of the G matrix as

$$C = \begin{bmatrix} G_{12}^{-1} & -G_{12}^{-1}G_{11} \\ G_{22}G_{21}^{-1} & G_{21} - G_{22}G_{12}^{-1}G_{11} \end{bmatrix}. \tag{3.94}$$

This new model corresponds to the block diagram in Fig. 3.32. Note however, that the diagram may seduce one to misinterpretation that we are reallocating the actuators and sensors in the system. No, it is only that we changed the "format" of its mathematical model. One should perhaps abandon the *input-output* viewpoint (that is why we used quotation marks with the terms inputs and outputs above) and view (3.93) as an *equation* and not an *assignment* (which is suggested by the block diagram).
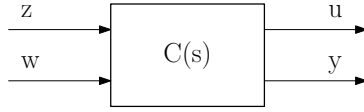

Figure 3.32: Block diagram for the chain matrix.

Note that with the background on the formats of models of two-port networks refreshed in this work, we can recognize the matrix C as the so-called *chain matrix* (the matrix B that we used extensively in this work was actually its inverse—the inverse chain matrix). Mapping it to the two-port setting, the matrix-vector relationship is

$$\begin{bmatrix} \hat{u}_1(s) \\ \hat{i}_1(s) \end{bmatrix} = \begin{bmatrix} C_{11}(s) & C_{12}(s) \\ C_{21}(s) & C_{22}(s) \end{bmatrix} \begin{bmatrix} \hat{u}_2(s) \\ \hat{i}_2(s) \end{bmatrix}. \tag{3.95}$$

Having such new model and the controller description

$$\hat{u}(s) = K(s)\,\hat{y}(s), \tag{3.96}$$

the same closed-loop transfer function considering w as its input and z as the output can be computed surprisingly conveniently. Upon substitution for u in (3.93) we get

$$\begin{bmatrix} \hat{z} \\ \hat{w} \end{bmatrix} = \begin{bmatrix} C_{11}\,K + C_{12} \\ C_{21}\,K + C_{22} \end{bmatrix} \hat{y}, \tag{3.97}$$

which yields the desired transfer function from w to z

$$\hat{z} = (C_{11}\,K + C_{12})(C_{21}\,K + C_{22})^{-1}\,\hat{w}. \tag{3.98}$$

Observe that the unknown K now appears in a different manner in the closed-loop transfer function. Note that similarly to (3.98), this is another instance of linear fractional transformation (also called *homographic transformation*).

With the new *format* of the model, different optimization procedures can be anticipated. The new model has been called *chain-scattering* representation in the control theory literature that we are going to reference. This makes reference to the concept of a *scattering* description of an LTI dynamical system (in fact, an N-port) introduced in late 1940s in the electrical circuits (called electrical networks back in the days) community (see the next section for references). It is now hard to trace who originally introduced this idea to the control theory community. Apparently, there were several researchers working on the topic in the late 1980s. Most probably the idea appeared first in one of Kimura's papers such as [33], [34]. Later in mid 1990s Kimura made the concept popular through [36] and in particular through his monograph [35].

Among other key early contributors were Hara [26] and Tsai [76] and [78]. The latter has recently published an update on the research in the domain [77].

In those works, no analysis of chains or ladders is actually made. Moreover, it is actually difficult to understand more intimate relationship with the concept of scattering (as introduced by electrical engineers) other than through the switch from the (inverse) hybrid model to the (inverse) chain model by swapping the causality of one input-output pair. Indeed, in [35], page 73, Example 4.1, an electrical two-port circuits is considered, characterized by two voltage-current pairs, one combination of inputs and outputs is (correctly) called *hybrid description* whereas the other is (incorrectly) called *chain scattering representation*. But true scattering (as introduced by electrical engineers), hence also chain scattering, involves transformation of physical variables in the first place. Instead of voltages and currents, voltage waves or current waves or power waves are used. That is why I am still not able to map my own results to the results that claim to make use of (chain) scattering framework in the controls literature.

3.10.2 Wave transfer functions for lumped chains by O'Connor

One of the primary motivations for the presented research was to understand better the how the concept of *wave transfer function* (WTF) as promoted by O'Connor [59] relates to the established theories. Now that we have exposed the general control design methodology based on the concept of impedance matching, it is time to see how it relates the the WTF methodology. For convenience of the readers, we go through a mini intro to that methodology based on the above mentioned paper.

The position of the k-th particle of mass m in the chain is labeled as x_k. In the simplest case, a uniform chain is considered. Assuming temporarily that the chain has no beginning and no end, the global behavior can be captured by a local model

$$\hat{x}_{k+1}(s) = G(s)\hat{x}_k(s), \tag{3.99}$$

where the hat denotes a Laplace transform of the corresponding time-domain variable. It also immediately follows that

$$\hat{x}_{k+n}(s) = G^n(s)\hat{x}_k(s), \tag{3.100}$$

It may come as a surprise that the model only contains a one-directional coupling while the physics of the problem is certainly bidirectional. But the bidirectionality is hidden in the suitable choice of the transfer function G. The equation of motion is

$$m\ddot{x}_k(t) = k\left(x_{k-1}(t) - 2x_k(t) + x_{k+1}\right). \tag{3.101}$$

Substituting (3.99) into (3.101), we get

$$ms^2\hat{x}_k(s) = k\hat{x}_k(s)(G^{-1}(s) - 2 + G(s)). \tag{3.102}$$

Multiplying both sides by G we get a quadratic (in G) equation

$$k\,G^2 - (2k + ms^2)\,G + k\,G^2 = 0. \tag{3.103}$$

The equation has two solution

$$G_{\mathrm{a}}(s) = 1 + \frac{1}{2}\left(\frac{s}{\omega_n}\right)^2 - \frac{s}{\omega_n}\sqrt{1 + \left(\frac{s}{2\omega_n}\right)^2} \tag{3.104}$$

$$G_{\mathrm{b}}(s) = 1 + \frac{1}{2}\left(\frac{s}{\omega_n}\right)^2 + \frac{s}{\omega_n}\sqrt{1 + \left(\frac{s}{2\omega_n}\right)^2}, \tag{3.105}$$

where

$$\omega_n = \sqrt{\frac{k}{m}}. \tag{3.106}$$

The frequency responses corresponding to the two transfer function are in Fig. 3.33a and 3.33b.

The similarity with the results presented earlier in this chapter catches an eye. Namely, G_{a} and G_{b} are identical with the two eigenvalues λ_1 and λ_2 (3.22) of the (inverse) chain matrix B (3.20) of a single section of the ladder, respectively.

Now, of the two transfer functions, only G_{a} corresponds to a causal system. It is argued in [58] that the position $x_k(t)$ of each particle in the chain can be decomposed into two parts

$$x_k(t) = a_k(t) + b_k(t) \tag{3.107}$$

such that their Laplace transforms of the two components satisfy

$$\hat{a}_{k+1}(s) = G_a\hat{a}_k(s) \tag{3.108}$$

(a) G_a

(b) G_b
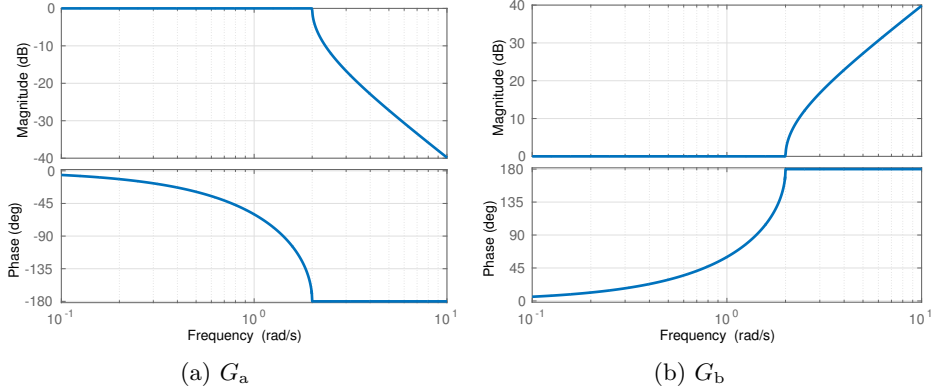
Figure 3.33: Magnitude and phase frequency responses for the two wave transfer functions

and

$$\hat{b}_{k+1}(s) = G_b(s)\hat{b}_k(s) \tag{3.109}$$

$$= G_a^{-1}(s)\hat{b}_k(s), \tag{3.110}$$

which can be turned into a causal relationship

$$\hat{b}_k(s) = G_a(s)\hat{b}_{k+1}(s). \tag{3.111}$$

Since we will only use the causal transfer function, let's relabel it into G for the same of notational simplicity

$$G(s) \coloneqq G_a(s). \tag{3.112}$$

This can invoke the idea of viewing $a_k(t)$ as the forward (towards the right end) traveling component of the position $x_k(t)$ and $b_k(t)$ as the backward traveling component (away from the right end).

The Laplace transform of the position $x_k(t)$ can therefore be written as

$$\hat{x}_k(s) = G(s)\hat{a}_{k-1}(s) + G(s)\hat{b}_{k+1}(s). \tag{3.113}$$

Now, for a finite-length chain whose first (the leftmost) particle's position is set by the actuator and the last (the rightmost) particle is freely floating, a signal-flow diagram is in Fig. 3.34 (as given in [58]).

If no compensation is designed and implemented, each commanded change in the actuator's position $x_0(t)$ triggers a wave which travels towards the right end,
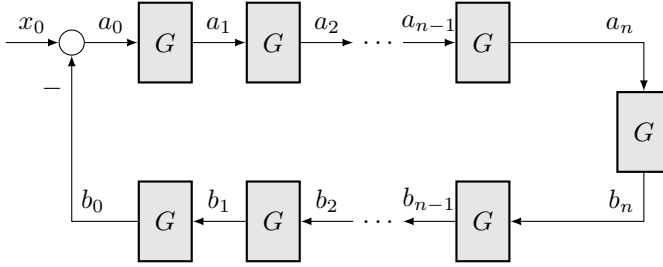
Figure 3.34: Signal-flow diagram for the wave transfer function modeling

gets reflected and then travels backwards towards the actuator, then subtracts from the actuator's action and, provided no dissipation is in the chain, a nev-erending cycle appears. This is how the rise of standing waves can be viewed. In [58] a compensation scheme is proposed: first, estimate the traveling wave com-ponent $b_0(t)$ arriving at the actuator's side of the chain and subtracting from the actuator's action; second, build a signal that approximates this incoming wave and *add* it to the actuator command. Hence, an active compensation scheme.

In order to estimate the incoming wave $b_0(t)$, one more (but only one more) particle's position (say, x_k) needs to be measured and the wave transfer function (WTF) $G(s)$ needs to be approximately implemented as a real-time filter. Typ-ically, standard second-order LTI filter suffices. The resulting compensators has this transfer function model

$$\hat{b}_0(s) = \left[-\frac{G^2(s)}{1-G^2(s)} \quad \frac{G(s)}{1-G^2(s)} \right] \begin{bmatrix} \hat{x}_0(s) \\ \hat{x}_1(s) \end{bmatrix}. \tag{3.114}$$

Now, let's compare this with the impedance matching compensation scheme studied in this work (see the signal flow diagram in Fig. 3.9): the concept of iterative impedance (or matching impedance) offers two "controllers" that can be implemented on one or both sides. One solution is passive, the other one is active. The passive component dissipates just the right amount of energy so no (or little) is reflected back. The active solution, on the other hand, lets the incoming wave to reflect but it generates an output that acts in the opposite sense, hence an active compensation.

3.11 Conclusions and further research

In this chapter we analyzed the problem of determining iterative impedances in lossless ladders formed by sections composed of L and C elements, while our

motivation was to find analogies to these results in other physical domains. We learned that the iterative impedances play the role of reflection-free matching impedances well known from transmission lines. We formulated this design problem in the popular LFT framework and showed that this leads to a nontraditional control design assignment in which a controller needs to be designed such that the transfer function of the closed-loop is identical to that of the controller. An interesting property of this controller is that it does not depend on the number of sections. It works perfectly well for one or one hundred sections. On the other hand, the controller is described by an irrational transfer function. Finally, we analyzed how the standard $\mathcal{H}_\infty$-optimal controller relates to this nontraditional impedance matching controller. We showed that for a ladder of growing number of sections, the irrational impedance matching controller is a good approximation to the rational $\mathcal{H}_\infty$-optimal controller, whose order grows with the number of sections. We also strove to interpret this result as a reformulation of the *wave transfer function* approach proposed in the literature.

The final message of the whole presented work is that the multiport framework, and in particular the scattering description, developed several decades ago for description, analysis and synthesis of electrical networks, both passive and active, may be quite useful even in other physical domains. Of particular interest might be further investigation of the relationship between asymmetry of coupling, reciprocity and activeness (the opposite of passivity) of dynamical systems.

Bibliography

[1] Brian D. O. Anderson and Sumeth Vongpanitlerd. *Network Analysis and Synthesis: A Modern Systems Theory Approach*. Dover Publications, October 2006.

[2] R. Anderson and M.W. Spong. Bilateral control of teleoperators with time delay. *IEEE Transactions on Automatic Control*, 34(5):494–501, May 1989.

[3] M. Arcak. Passivity as a Design Tool for Group Coordination. *IEEE Transactions on Automatic Control*, 52(8):1380–1390, August 2007.

[4] Petr Augusta and Zdeněk Hurák. Distributed stabilisation of spatially invariant systems: positive polynomial approach. *Multidimensional Systems and Signal Processing*, pages 1–19, 2013.

[5] Norman Balabanian and Theodore Bickart. *Linear Network Theory: Analysis, Properties, Design and Synthesis*. Matrix Pub, Beaverton, Or., February 1982.

[6] B. Bamieh, F. Paganini, and M.A. Dahleh. Distributed control of spatially invariant systems. *IEEE Transactions on Automatic Control*, 47(7):1091–1107, 2002.

[7] V. Belevitch. *Classical Network Theory*. Holden-Day, 1968.

[8] Vitold Belevitch. Transmission Losses in 2n-Terminal Networks. *Journal of Applied Physics*, 19(7):636–638, July 1948.

[9] Peter C. Breedveld and Hogan Neville. The Physical Basis of Analogies in Physical System Models. In *The Mechatronics Handbook - 2 Volume Set*, Mechatronics Handbook 2e. CRC Press, 2002.

[10] Forbes T. Brown. *Engineering System Dynamics: A Unified Graph-Centered Approach, Second Edition*. CRC Press, 2 edition, August 2006.

[11] Izhak Bucher. Traveling waves: Signal processing, control, modeling, identification, dynamics and applications in mechanics and engineering. *Mechanical Systems and Signal Processing*, 39(1–2):1–2, August 2013.

Bibliography

[12] Kai-ching Chu. Decentralized Control of High-Speed Vehicular Strings. *Transportation Science*, 8(4):361–384, November 1974.

[13] Leon O Chua, Charles A Desoer, and Ernest S Kuh. *Linear and nonlinear circuits*. McGraw-Hill, New York, 1987.

[14] Robert L. Cosgriff. The Asymptotic Approach to Traffic Dynamics. *IEEE Transactions on Systems Science and Cybernetics*, 5(4):361–368, 1969.

[15] Ruth F. Curtain and Hans Zwart. *An Introduction to Infinite-Dimensional Linear Systems Theory*. Springer, 2012.

[16] Charles A Desoer and Ernest S Kuh. *Basic circuit theory*. McGraw-Hill, New York, 1969.

[17] R. H. Dicke. A Computational Method Applicable to Microwave Networks. *Journal of Applied Physics*, 18(10):873–878, October 1947.

[18] O. Egeland and J.T. Gravdahl. *Modeling and simulation for automatic control*. Marine Cybernetics, 2002.

[19] J.P. Epperlein, B. Bamieh, and K.J. Astrom. Thermoacoustics and the Rijke Tube: Experiments, Identification, and Modeling. *IEEE Control Systems*, 35(2):57–77, April 2015.

[20] J.A. Fax and R.M. Murray. Information flow and cooperative control of vehicle formations. *IEEE Transactions on Automatic Control*, 49(9):1465–1476, 2004.

[21] Ciprian Foias, Hitay Özbay, Allen Tannenbaum, and & 0 more. *Robust Control of Infinite Dimensional Systems: Frequency Domain Methods*. Springer, London ; New York, December 1995.

[22] P.J. Gawthrop and G.P. Bevan. Bond-graph modeling. *IEEE Control Systems*, 27(2):24–45, 2007.

[23] Y. Halevi. On control of flexible structures. In *Proceedings of the 41st IEEE Conference on Decision and Control, 2002*, volume 1, pages 232–237 vol.1, December 2002.

[24] Y. Halevi and C. Wagner-Nachshoni. Feedback control of flexible structures with non-uniform rods. In *American Control Conference, 2003. Proceedings of the 2003*, volume 3, pages 2646–2651 vol.3, June 2003.

[25] Yoram Halevi. Control of Flexible Structures Governed by the Wave Equation Using Infinite Dimensional Transfer Functions. *Journal of Dynamic Systems, Measurement, and Control*, 127(4):579–588, December 2004.

[26] S. Hara and R. Kondo. Characterization and computation of H_infinity-optimal controllers in the state-space. In *Proceedings of the 27th IEEE Conference on Decision and Control*, pages 20–25 vol.1, December 1988.

[27] I. Herman, D. Martinec, Z. Hurak, and M. Sebek. Nonzero Bound on Fiedler Eigenvalue Causes Exponential Growth of H-Infinity Norm of Vehicular Platoon. *IEEE Transactions on Automatic Control*, 60(8):2248–2253, August 2015.

[28] Ivo Herman, Dan Martinec, Zdeněk Hurák, and Michael Sebek. Scaling in bidirectional platoons with dynamic controllers and proportional asymmetry. *arXiv:1410.3943 [cs]*, October 2014. arXiv: 1410.3943.

[29] Peter F. Hokayem and Mark W. Spong. Bilateral teleoperation: An historical survey. *Automatica*, 42(12):2035–2057, December 2006.

[30] Z. Hurak and J. Zemanek. Feedback linearization approach to distributed feedback manipulation. In *American Control Conference (ACC), 2012*, pages 991–996, 2012.

[31] Zdenek Hurak and Michael Sebek. 2d polynomial approach to stability of platoons of vehicles. In *Proceedings of the 2nd IFAC Workshop on Distributed Estimation and Control in Networked Systems*, volume 2, Centre de Congrès de L'Impérial Palace, Annecy, France, 2010.

[32] Dean Karnopp, Donald L Margolis, and Ronald C Rosenberg. *System dynamics modeling, simulation, and control of mechatronic systems*. John Wiley & Sons, Hoboken, N.J., 5 edition, 2012.

[33] Hidenori Kimura. Conjugation and model-matching in $H \infty$. In *Proceedings of the 27th IEEE Conference on Decision and Control*, pages 979–984 vol.2, December 1988.

[34] Hidenori Kimura. Linear fractional transformations and J-lossless factorization in H-infinity control theory. In *American Control Conference, 1990*, pages 3085–3091, May 1990.

[35] Hidenori Kimura. *Chain-Scattering Approach to H-infinity-Control*. Birkhäuser Boston, 1 edition, December 1996.

[36] Hidenori Kimura and Fumitake Okunishi. Chain-Scattering Approach to Control System Design. In Professor Alberto Isidori, editor, *Trends in Control*, pages 151–171. Springer London, January 1995.

[37] Ernest S. Kuh. *Theory of Linear Active Networks*. Holden-Day, Inc., 1 edition, 1967.

Bibliography

[38] K. Kurokawa. Power Waves and the Scattering Matrix. *IEEE Transactions on Microwave Theory and Techniques*, 13(2):194–202, March 1965.

[39] K. Kurokawa. *Introduction to the Theory of Microwave Circuits*. Academic Press, New York, 1st ed. edition edition, 1969.

[40] B.C. Lesieutre, E. Scholtz, and George C. Verghese. Impedance matching controllers to extinguish electromechanical waves in power networks. In *Proceedings of the 2002 International Conference on Control Applications, 2002*, volume 1, pages 25–30, 2002.

[41] W.S. Levine and M. Athans. On the optimal error regulation of a string of moving vehicles. *IEEE Transactions on Automatic Control*, 11(3):355–361, 1966.

[42] Philip Cooper Magnusson. *Transmission lines and wave propagation*. CRC Press, Boca Raton, FL, 2001.

[43] I.A. Maio. A primer on scattering parameters, Part I: Definitions and properties. *IEEE EMC Newsletter*, pages 57–63, 2008.

[44] D. Martinec and Z. Hurak. Vehicular platooning experiments with LEGO MINDSTORMS NXT. In *2011 IEEE International Conference on Control Applications (CCA)*, pages 927–932, September 2011.

[45] D. Martinec, M. Sebek, and Z. Hurak. Vehicular platooning experiments with racing slot cars. In *2012 IEEE International Conference on Control Applications (CCA)*, pages 166–171, 2012.

[46] Dan Martinec, Ivo Herman, Zdeněk Hurák, and Michael Šebek. Wave-absorbing vehicular platoon controller. *European Journal of Control*, 20(5):237–248, September 2014.

[47] A. Megretski and A. Rantzer. System analysis via integral quadratic constraints. *IEEE Transactions on Automatic Control*, 42(6):819–830, 1997.

[48] S. M. Melzer and B. Kuo. A closed-form solution for the optimal error regulation of a string of moving vehicles. *IEEE Transactions on Automatic Control*, 16(1):50–52, 1971.

[49] Giovanni Miano and Antonio Maffucci. *Transmission lines and lumped circuits*. Academic Press, San Diego, 2001.

[50] D.W. Miller and A. von Flotow. A travelling wave approach to power flow in structural networks. *Journal of Sound and Vibration*, 128(1):145–162, January 1989.

[51] Carol Gray Montgomery, Robert Henry Dicke, and Edward M. Purcell. *Principles of Microwave Circuits*. IET, 1948.

[52] K. Nagase, H. Ojima, and Y. Hayakawa. Wave-based Analysis and Wave Control of Ladder Networks. In *44th IEEE Conference on Decision and Control, 2005 and 2005 European Control Conference. CDC-ECC '05*, pages 5298–5303, 2005.

[53] Kenji Nagase, Hirotaka Ojima, and Yoshikazu Hayakawa. Wave control of multi-story structures by active mass dampers. *Proceedings of the International Conference on Motion and Vibration Control*, 6(2):702–709, 2002.

[54] Robert W. Newcomb. *Linear Multiport Synthesis*. McGraw-Hill, 1966.

[55] William J. O'Connor. A Gantry Crane Problem Solved. *Journal of Dynamic Systems, Measurement, and Control*, 125(4):569–576, January 2004.

[56] William J. O'Connor. Wave-echo position control of flexible systems: towards an explanation and theory. In *American Control Conference, 2004. Proceedings of the 2004*, volume 5, pages 4837–4842 vol.5, June 2004.

[57] William J. O'Connor. Wave-echo control of lumped flexible systems. *Journal of Sound and Vibration*, 298(4–5):1001–1018, December 2006.

[58] William J. O'Connor. Control of flexible mechanical systems: wave-based techniques. In *American Control Conference, 2007. ACC '07*, pages 4192–4202, July 2007.

[59] William J. O'Connor. Wave-Based Analysis and Control of Lump-Modeled Flexible Robots. *IEEE Transactions on Robotics*, 23(2):342–352, April 2007.

[60] William J. O'Connor and Alessandro Fumagalli. Refined Wave-Based Control Applied to Nonlinear, Bending, and Slewing Flexible Systems. *Journal of Applied Mechanics*, 76(4):041005–041005, April 2009.

[61] William J. O'Connor and Donogh Lang. Position Control of Flexible Robot Arms Using Mechanical Waves. *Journal of Dynamic Systems, Measurement, and Control*, 120(3):334–339, September 1998.

[62] William J. O'Connor, Francisco Ramos de la Flor, David J. McKeown, and Vicente Feliu. Wave-based control of non-linear flexible mechanical systems. *Nonlinear Dynamics*, 57(1-2):113–123, July 2009.

[63] William J. O'Connor and Ming Zhu. Boundary-controlled travelling and standing waves in cascaded lumped systems. *Mechanical Systems and Signal Processing*, 39(1–2):119–128, August 2013.

Bibliography

[64] William J. O'Connor and Ming Zhu. Travelling waves in boundary-controlled, non-uniform, cascaded lumped systems. *Mechanical Systems and Signal Processing*, 39(1–2):108–118, August 2013.

[65] H. Ojima, K. Nagase, and Y. Hayakawa. Wave-based analysis and wave control of damped mass-spring systems—characterization from the propagation contants. *Transactions of the Society of Instrument and Control Engineers*, 38(3):239–246, 2002.

[66] Henry Martyn Paynter. *Analysis and Design of Engineering Systems: Class Notes for M.I.T. Course 2.751*. M.I.T. Press, 1961.

[67] I. Peled, W. J. O'Connor, and Y. Halevi. On the relationship between wave based control, absolute vibration suppression and input shaping. *Mechanical Systems and Signal Processing*, 39(1–2):80–90, August 2013.

[68] L. Peppard. String stability of relative-motion PID vehicle control systems. *IEEE Transactions on Automatic Control*, 19(5):579–581, 1974.

[69] David M Pozar. *Microwave engineering*. Wiley, Hoboken, NJ, 2012.

[70] J. Rahola. Power Waves and Conjugate Matching. *IEEE Transactions on Circuits and Systems II: Express Briefs*, 55(1):92–96, January 2008.

[71] P. Seiler, A. Pant, and K. Hedrick. Disturbance propagation in vehicle strings. *IEEE Transactions on Automatic Control*, 49(10):1835–1842, 2004.

[72] A. Semlyen. Analysis of Disturbance Propagation in Power Systems Based on a Homogeneoue Dynamic Model. *IEEE Transactions on Power Apparatus and Systems*, PAS-93(2):676–684, March 1974.

[73] William Singhose. Command shaping for flexible systems: A review of the first 50 years. *International Journal of Precision Engineering and Manufacturing*, 10(4):153–168, October 2009.

[74] L. Sirota and Y. Halevi. Wave based vibration control of membranes. In *American Control Conference (ACC), 2014*, pages 2729–2734, June 2014.

[75] J.S. Thorp, C.E. Seyler, and A.G. Phadke. Electromechanical wave propagation in large electric power systems. *IEEE Transactions on Circuits and Systems I: Fundamental Theory and Applications*, 45(6):614–622, 1998.

[76] M.-C. Tsai and C.-S. Tsai. A chain scattering-matrix description approach to H_infinity control. *IEEE Transactions on Automatic Control*, 38(9):1416–1421, September 1993.

[77] Mi-Ching Tsai and Da-Wei Gu. *Robust and Optimal Control: A Two-port Framework Approach.* Springer, New York, 2014 edition edition, January 2014.

[78] Mi-Ching Tsai and Ian Postlethwaite. On J-Lossless coprime factorizations and H-infinity control. *International Journal of Robust and Nonlinear Control*, 1(1):47–68, 1991.

[79] D.R. Vaughan. Application of Distributed Parameter Concepts to Dynamic Analysis and Control of Bending Vibrations. *Journal of Basic Engineering*, 90(2):157–166, 1968.

[80] A.H. von Flotow. Disturbance propagation in structural networks. *Journal of Sound and Vibration*, 106(3):433–450, May 1986.

[81] A.H. von Flotow. Traveling wave control for large spacecraft structures. *Journal of Guidance, Control, and Dynamics*, 9(4):462–468, July 1986.

[82] A.H. von Flotow. Research into Traveling Wave Control in Flexible Structures. Final report, Department of Aeronautics and Astronautics Massachusetts Institute of Technology, 1990.

[83] John A. Wheeler. On the Mathematical Description of Light Nuclei by the Method of Resonating Group Structure. *Physical Review*, 52(11):1107–1122, December 1937.

[84] D. Williams. Traveling Waves and Power Waves: Building a Solid Foundation for Microwave Circuit Theory. *IEEE Microwave Magazine*, 14(7):38–45, November 2013.

[85] D.C. Youla. A tutorial exposition of some key network-theoretic ideas underlying classical insertion-loss filter design. *Proceedings of the IEEE*, 59(5):760–799, May 1971.

[86] Jiří Zemánek, Tomáš Michálek, and Zdeněk Hurák. Feedback control for noise-aided parallel micromanipulation of several particles using dielectrophoresis. *ELECTROPHORESIS*, 36(13):1451–1458, 2015.

[87] Kemin Zhou, John C. Doyle, and Keith Glover. *Robust and Optimal Control.* Prentice Hall, 1 edition, August 1995.